

ARL 66-0141

JULY 1966



Aerospace Research Laboratories

BOUNDARY LAYER PROFILE MEASUREMENTS IN HYPERSONIC NOZZLES

NORMAN E. SCAGGS

FLUID DYNAMICS FACILITIES RESEARCH LABORATORY

PROJECT 7065

Distribution of this document is unlimited.

APR 27 1967

OFFICE OF AEROSPACE RESEARCH
United States Air Force

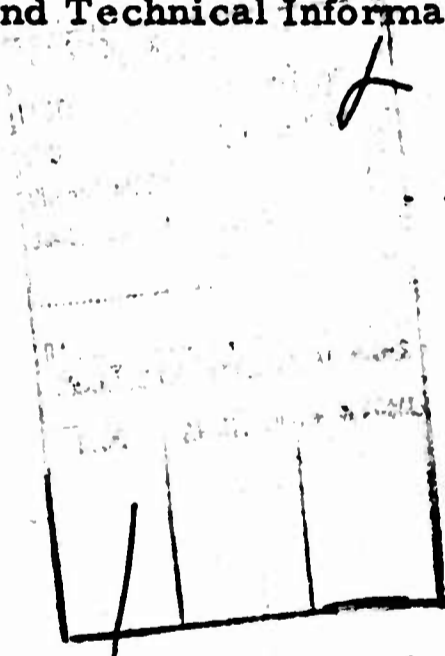
ARCHIVE COPY



NOTICES

When Government drawings, specifications, or other data are used for any purpose other than in connection with a definitely related Government procurement operation, the United States Government thereby incurs no responsibility nor any obligation whatsoever; and the fact that the Government may have formulated, furnished, or in any way supplied the said drawings, specifications, or other data, is not to be regarded by implication or otherwise as in any manner licensing the holder or any other person or corporation, or conveying any rights or permission to manufacture, use, or sell any patented invention that may in any way be related thereto.

Qualified requesters may obtain copies of this report from the Defense Documentation Center, (DDC), Cameron Station, Alexandria, Virginia. All others should apply to the Clearinghouse for Scientific and Technical Information.



Copies of ARL Technical Documentary Reports should not be returned to Aerospace Research Laboratories unless return is required by security considerations, contractual obligations or notices on a specified document.

ARL 66-0141

**BOUNDARY LAYER PROFILE MEASUREMENTS
IN HYPERSONIC NOZZLES**

*NORMAN E. SCAGGS
FLUID DYNAMICS FACILITIES RESEARCH LABORATORIES*

PROJECT 7065

JULY 1966

**Distribution of this
document is unlimited**

**AEROSPACE RESEARCH LABORATORIES
OFFICE OF AEROSPACE RESEARCH
UNITED STATES AIR FORCE
WRIGHT-PATTERSON AIR FORCE BASE, OHIO**

FOREWORD

This technical report was prepared by Norman E. Scaggs, Fluid Dynamics Facilities Research Laboratory of the Aerospace Research Laboratories, Wright-Patterson Air Force Base, Ohio. The work reported was accomplished under Project 7065, "Aerospace Simulation Techniques Research, " and in partial fulfillment of the requirements for the degree of master of science.

The author wishes to express his gratitude to Dr. John. D. Lee of the Ohio State University who conceived this investigation and whose direction and helpful advice made possible the completion of this task. The author also wishes to thank the staff of the Aerodynamic Laboratory of the Ohio State University for their cooperation and assistance in the conduction of the experiments.

ABSTRACT

An experimental investigation made to determine the flow parameter profiles across the boundary layer on contoured, axisymmetric hypersonic nozzles is described. The pitot pressure and total temperature profiles measured across the boundary layers on nozzles of Mach number seven and twelve are shown in graphical form. The static temperature and velocity profiles, calculated with the assumption of constant static pressure across the boundary layer, are given. A correlation is shown to exist between the exponent of the velocity profile power law and the product of the ratios of wall temperature to free stream total temperature and axial distance to momentum thickness. The static temperature profiles, calculated from the measured data is compared with Crocco's relationship for the static temperature in terms of the velocity profile.

TABLE OF CONTENTS

<u>SECTION</u>	<u>PAGE</u>
I INTRODUCTION	1
II EXPERIMENTS	
A. General	3
B. Measurement Techniques	3
III RESULTS AND DISCUSSION	9
IV CONCLUSIONS.....	14
REFERENCES	15
TABLE I — Composite Listing of Test Conditions and Resultant Parameters.....	16

LIST OF FIGURES

<u>FIGURE</u>	<u>PAGE</u>
1. Sonic-Pneumatic Probe Assembly	17
2. Calibration of Sonic-Pneumatic Probe	18
3. Schematic Diagram of a Sonic-Pneumatic Probe System	19
4. Caloric Imperfection Corrections	20
5. Mach Seven Nozzle	21
6. Mach Twelve Nozzle	22
7. Pitot Pressure Profiles at Mach 6.5	23
8. Pitot Pressure Profiles at Mach 11.5	24
9. Mach Number Profiles at Mach 6.5	25
10. Mach Number Profiles at Mach 11.5	26
11. Total Temperature Profiles at Mach 6.5	27
12. Total Temperature Profiles at Mach 11.5	28
13. Mach Number, Velocity, and Static Temp. Profiles	29
14. Mach Number, Velocity, and Static Temp. Profiles	30
15. Mach Number, Velocity, and Static Temp. Profiles	31
16. Mach Number, Velocity, and Static Temp. Profiles	32
17. Mach Number, Velocity, and Static Temp. Profiles	33
18. Mach Number, Velocity, and Static Temp. Profiles	34
19. Mach Number, Velocity, and Static Temp. Profiles	35
20. Mach Number, Velocity, and Static Temp. Profiles	36
21. Correlation of Velocity Profile Power Law Exponent	37
22. Comparison of Static Temperature Profile at Mach 6.5 ..	38
23. Comparison of Static Temperature Profile at Mach 11.5 .	39

SYMBOLS

A	area
V	velocity
T	temperature
P	pressure
M	Mach number
ρ	density
\dot{m}	mass flow rate
a	speed of sound
γ	ratio of specific heats
R	gas constant for air
K	constant in mass flow equation (B-4)
K₃	constant in the total temperature equation (B-9)
y	distance from nozzle wall
x	distance from nozzle throat along the nozzle centerline
n	reciprocal of the velocity profile power law exponent
θ	momentum thickness
δ^*	displacement thickness
δ	boundary layer thickness
Pr	Prandtl number
H	shape factor
Re_x	Reynolds number at the edge of the boundary layer based on distance from nozzle throat
Re_{θ}	Reynolds number at the edge of the boundary layer based on the momentum thickness
Re_{δ^*}	Reynolds number at the edge of the boundary layer based on the displacement thickness

Re_δ Reynolds number at the edge of the boundary layer based on the boundary layer thickness

D^* diameter of nozzle throat

SUBSCRIPTS

∞ free stream condition

0 stagnation condition

1 condition just upstream of first throat

2 condition just upstream of second throat

w condition at nozzle wall

(none) static condition within the boundary layer

SUPERSCRIPTS

* at the critical cross section (the choked throats of the sonic-pneumatic probe system and the nozzle throats) — except for δ^*

I. INTRODUCTION

The boundary layer growth on hypersonic nozzles is extremely important because it greatly affects the flow field produced by any physical wall contour. In order to design a nozzle to produce a given set of free stream conditions, a correction to the inviscid core coordinates must be made to allow for the boundary layer effects. In general the design of the nozzle is carried out by first calculating the inviscid core and then adding a displacement thickness correction at each station to obtain the final physical wall coordinate. The main difficulty in nozzle design is the accurate calculation of this displacement thickness correction.

There are several methods for calculating the displacement thickness growth, either by empirical methods or analytical methods, Reference (1-5). The analytical methods require assumptions about the flow parameter profiles (V , T , p , M) across the boundary layer. If the Mach number and two of the other parameters are known, then all of the flow parameters in the boundary layer can be calculated including the displacement thickness.

The purpose of this investigation was to make actual measurements of the flow parameters in the boundary layer on hypersonic nozzles in an effort to answer some of the questions about the variation of the parameters across the boundary layer. The experiments were carried out in two nozzles, one delivered a nominal Mach number of seven, the other delivered a nominal Mach number of twelve. The pitot pressure distribution and the total temperature distribution were measured across the boundary layer. The static pressure was assumed

to be constant across the boundary layer. These measured parameters were then used to calculate all the other flow parameters as well as displacement and momentum thicknesses.

One of the novel aspects of this investigation was the use of a sonic-pneumatic probe in conjunction with a pitot probe to measure the total temperature distribution. This type temperature probe has been used by other authors to measure exhaust temperatures from jet engines, Reference (8), and the boundary layer measurements on models, Reference (6) and (7), but as far as the author knows this is the first attempt to use such a probe on hypersonic nozzles where the boundary layers are very thick (of the order of one to two inches) and the possibility of probe interactions with the flow field is minimized.

II. EXPERIMENTS

A. General

This investigation was carried out in the twelve-inch hypersonic wind tunnel of the Aerodynamic Laboratory of The Ohio State University. The facility is described in detail in Reference (9). Two different nozzles were used for the experiments, one producing a nominal Mach number of seven, the other producing a nominal Mach number of twelve. The nozzles were contoured, axisymmetric type. The details of the nozzles are shown in Figs. 5 and 6.

Four surveys of the boundary layer were made in each nozzle. In the nominal Mach seven nozzle, two surveys were made 3.5 inches upstream of the nozzle exit at Reynolds numbers, Re_x of 0.71×10^6 and 2.24×10^6 , and two surveys were made 10.5 inches upstream of the nozzle exit at Reynolds numbers, Re_x of 0.66×10^6 and 2.05×10^6 . In the nominal Mach twelve nozzle, two surveys were made 4.5 inches upstream of the nozzle exit at Reynolds numbers, Re_x of 1.28×10^6 and 2.82×10^6 , and two surveys were made 12 inches upstream of the nozzle exit at Reynolds numbers, Re_x of 1.18×10^6 and 2.68×10^6 .

In all the tests, the pitot pressure distribution was measured, the total temperature distribution was measured, the wall temperature and wall static pressure were measured. The tunnel stagnation pressure and temperature were also measured.

B. Measurement Techniques

A combination pitot pressure and sonic-pneumatic probe was used to measure the pitot pressure distribution and the total temperature

distribution. A schematic of the combination probe is shown in Fig. 1. The design of the sonic-pneumatic probe is based on the results of Reference (10). It was shown in Reference (10) that it is possible to measure the total temperature in a hypersonic stream within $\pm 3\%$ of the true value within the temperature range of these tests.

The principle of the sonic-pneumatic probe is based on the application of the perfect gas law, the law of the conservation of mass, and Bernoulli's Theorem. Its operation is based on the principle of equal mass flow through two sonic orifices in series. The mass flow rate through a sonic orifice is given by:

$$\dot{m} = \rho^* a^* A^* \quad (B-1)$$

Now by the perfect gas law:

$$\rho^* = \frac{\rho^*}{\rho_0} \rho_0 = \frac{\rho^*}{\rho_0} \frac{P_0}{RT_0} \quad (B-2)$$

and:

$$a^{*2} = \gamma^* RT^* \quad (B-3)$$

Putting (B-2) and (B-3) into (B-1) gives:

$$\dot{m} = \frac{\rho^*}{\rho_0} \frac{P_0}{RT_0} \sqrt{\gamma^* RT^*} A^* = \frac{\rho^*}{\rho_0} \sqrt{\frac{T^*}{T_0}} \sqrt{\frac{\gamma^*}{R}} \frac{P_0}{T_0} A^* = K \frac{P_0}{\sqrt{T_0}} A^* \quad (B-4)$$

If two orifices are in series as shown in Fig. 3 and sufficient pressure ratio is maintained across each to ensure that both are choked, then the mass flow rate through the first orifice is:

$$\dot{m}_1 = K_1 \frac{P_{O_1}}{\sqrt{T_{O_1}}} A_1^* \quad (B-5)$$

and the mass flow rate through the second orifice is:

$$\dot{m} = K_2 \frac{P_{O_2}}{\sqrt{T_{O_2}}} A_2^* \quad (B-6)$$

Now by the principle of the conservation of mass, the mass flow rate through the first orifice is equal to the mass flow rate through the second orifice.

Thus:

$$\dot{m}_1 = \dot{m}_2 \quad (B-7)$$

or equating equations (B-5) and (B-6)

$$K_1 \frac{P_{O_1}}{\sqrt{T_{O_1}}} A_1^* = K_2 \frac{P_{O_2}}{\sqrt{T_{O_2}}} A_2^* \quad (B-8)$$

Now solving for T_{O_1} :

$$T_{O_1} = \left(\frac{K_1}{K_2} \right)^2 \left(\frac{P_{O_1}}{P_{O_2}} \right)^2 \left(\frac{A_2^*}{A_1^*} \right)^{-2} T_{O_2} = K_3 \left(\frac{P_{O_1}}{P_{O_2}} \right)^2 \left(\frac{A_2^*}{A_1^*} \right)^{-2} T_{O_2} \quad (B-9)$$

A plot of K_3 versus total temperature from Reference (11) is shown in Fig. 4. For this series of tests, K_3 varies from .966 to 1.000 and since an iteration process would be required if these corrections were made, a value of $K_3 = 1.00$ was assumed throughout the data reduction. So the final equation is:

$$T_{O_1} = \left(\frac{P_{O_1}}{P_{O_2}} \right)^2 \left(\frac{A_2^*}{A_1^*} \right)^{-2} T_{O_2} \quad (B-10)$$

In this series of tests, P_{O_1} , P_{O_2} , and T_{O_2} were measured at each point in the boundary layer, so the only thing left undetermined was the ratio, $\frac{A_2^*}{A_1^*}$. If $\frac{A_2^*}{A_1^*}$ were simply the physical area ratio of the two orifices, then everything would be known; however, the effective area in each throat is decreased by the boundary layer established there by the flow through the sonic-pneumatic probe. The boundary layer thickness is a function of the flow conditions at each throat and, therefore, $\frac{A_2^*}{A_1^*}$ must be determined by a calibration. The calibration must be performed where the total temperature, T_{O_1} , upstream of the first throat is known.

Before this series of tests were conducted, a calibration of the probe was made in the same nozzles as the experiments were made but the probe was kept in the isentropic core. In the isentropic core the stagnation temperature upstream of the first orifice is equal to the tunnel stagnation temperature. Thus, T_{O_1} , T_{O_2} , P_{O_1} , and P_{O_2} are all known and $\left(\frac{A_2^*}{A_1^*} \right)$ is determined from the following equation:

$$\left(\frac{A_2^*}{A_1^*} \right)^{-2} = \frac{\frac{T_{O_1}}{T_{O_2}}}{\left(\frac{P_{O_1}}{P_{O_2}} \right)^2} \quad (B-11)$$

Equation (B-11) is a rearrangement of equation (B-10). The tunnel stagnation conditions were varied to obtain a range of upstream conditions for the first orifice and the results of the calibration were plotted versus the Reynolds number of the first orifice. Fig. 2 shows the results of the calibration. With the area ratio now determined as a function of the first orifice Reynolds number, T_{O_1} can be determined at any point in the boundary layer. An iteration process is required since the exact Reynolds number of the first orifice is not known until the exact total temperature upstream of the first orifice is known. This does not require a great number of calculations if the determination of T_{O_1} is started from the free stream edge of the boundary layer where T_{O_1} is known and continued toward the nozzle wall. Three iterations were usually sufficient to determine T_{O_1} .

P_{O_1} was sensed by a 0 — 2.0 PSID variable reluctance transducer, P_{O_2} was sensed by a 0 — 0.1 PSID variable reluctance transducer. T_{O_2} was sensed by a chromel — alumel bare wire thermocouple and recorded on a Brown Recorder. The pressures were recorded by the printer on the laboratory's analog computer described in Reference (9). The tunnel stagnation pressure was measured with a Laboratory Test Gage having an accuracy of 0.25 per cent of the gage range. The tunnel stagnation temperature was measured with a Type S (platinum - platinum rhodium) thermocouple and recorded on a Brown self-balancing potentiometer. The nozzle wall temperatures were measured with Type T thermocouples and recorded on a Brown self-balancing potentiometer. The nozzle wall static pressures were measured on a

silicone manometer tilted to thirty degrees from the horizontal. The instrumentation for the laboratory and the wind tunnel is discussed in more detail in Reference (9).

III. RESULTS

One of the first requirements in the reduction and analyzation of the data was the determination of the actual boundary layer thickness. Probably the most logical method was to look at the total temperature or velocity profiles and choose the boundary layer thickness where these parameters reached some percentage, such as ninety-nine per cent of free stream value. But this method does not work very well in a hypersonic nozzle since both these parameters are very close to ninety-nine per cent of free stream values over a large portion of the boundary layer and thus a wide range of values could be chosen for the boundary layer thickness. A different method was used in this investigation to determine the boundary layer thickness. This method involved the pitot pressure profiles and the edge of the boundary layer was chosen as the point where the pitot pressure gradient, $\frac{dp_{01}}{dy}$, was equal to zero.

Another decision that had to be made before the data could be reduced was what value of the static pressure across the boundary layer to use in the calculation of the Mach number distribution and the density distribution. Measurements of the wall static pressure opposite the axial position of the probe were made for each test. These values were compared to the free stream static pressure calculated from the Mach number at the edge of the boundary layer and the tunnel stagnation conditions. In all cases the wall static pressure was approximately ten per cent higher than the calculated free stream value. However, since these values were of the order of 0.01 PSIA,

it was assumed that the free stream value was correct and that some deficiency in the measuring technique allowed the indicated higher values. The free stream static pressure at the edge of the boundary layer was used in the data reduction.

The pitot pressure distributions for the Mach seven nozzle are shown in Fig. 7 and for the Mach twelve nozzle in Fig. 8. The profiles do not seem to be affected by the free stream Reynolds number but do tend to become fuller as the Mach number and the boundary layer thickness decrease.

The Mach number profiles are shown in Fig. 9 for the Mach seven nozzle and in Fig. 10 for the Mach twelve nozzles. These profiles naturally exhibit the same trends as the pitot pressure profiles. The Mach number profiles were calculated by using the tables of Reference (11) for the ratio of static pressure to pitot pressure versus Mach number.

The total temperature profiles, shown in Figs. 11 and 12, seemed to be affected by both the free stream Reynolds number, Re_x , and the temperature ratio, $\frac{T_w}{T_{O_{1\infty}}}$. T_w is the wall temperature

and $T_{O_{1\infty}}$ is the total temperature of the free stream at the edge of the boundary layer. The profiles become fuller as both the temperature ratio and the free stream Reynolds number increase.

Even though data was taken all the way to the wall until the probe touched, some of the data nearest the wall was discarded. Two criteria were used to eliminate some of the data. One criterion was when the centerline of the probe was within one probe tip diameter

(0.063 inches) of the wall. The other criterion was the pressure ratio, $\frac{P_{01}}{P_{02}}$. When this ratio became less than five, there was suspicion that the first throat was unchoked thus invalidating the data. Using these two limits for the data, the profiles extend only to approximately $\frac{y}{\delta}$ values of 0.2. To probe the flow nearer to the wall than this, a much smaller sonic-pneumatic probe would have to be used.

With the Mach number and total temperature profiles now available, the velocity profiles and the static temperature profiles were calculated. The static temperature at each location was calculated by using the tables of Reference (11) for the ratio of static temperature to total temperature for the measured Mach number and total temperature. The velocity at a given point was calculated using the equation:

$$V = M \sqrt{\gamma RT}$$

where T is the static temperature and M is the Mach number at a particular point. The velocity and static temperature profiles are shown in Figs. 13 through 20. The Mach number profiles are also included on these figures.

In order to correlate the velocity profiles with each other, an exponential curve of the form:

$$\frac{V}{V_{\infty}} = \left(\frac{y}{\delta} \right)^{\frac{1}{n}}$$

was fitted through the velocity profile points and an n determined. The values of n varied from 3.31 to 7.49 for all the test conditions.

A correlation was found to exist for the n 's of the form:

$$n = k \left(\frac{T_w}{T_{O_{1\infty}}} \right) \left(\frac{x}{\theta} \right)$$

where k is a constant, $\frac{T_w}{T_{O_{1\infty}}}$ is the ratio of the wall temperature to the free stream total temperature, x is the distance from the nozzle throat along the axis of symmetry, and θ is the momentum thickness. Fig. 21 illustrates this correlation. In Reference (3), a correlation of n versus Re_θ is made for experimental data from several investigators. There is considerable scatter in the data with points deviating from a mean line drawn through the data by as much as plus or minus twenty per cent. The data from the present investigation falls within this range of variation, but it seemed reasonable that a better correlation could be made by using a parameter that includes the heat transfer effects. The parameter, $\left(\frac{T_w}{T_{O_{1\infty}}} \right) \left(\frac{x}{\theta} \right)$, includes this effect and the correlation is much better as shown in Fig. 21 where the scatter is less than plus or minus ten per cent.

An attempt was also made to compare the static temperature profiles with the Crocco Relationship for the static temperature in terms of the velocity profile. Crocco's Relationship has the following form:

$$\frac{T}{T_{O_{1\infty}}} = \frac{T_w}{T_{O_{1\infty}}} - \left(\frac{T_w - T_{aw}}{T_{O_{1\infty}}} \right) \left(\frac{V}{V_\infty} \right) - \left(\frac{T_{aw} - T_\infty}{T_{O_{1\infty}}} \right) \left(\frac{V}{V_\infty} \right)^2$$

where

$$T_{aw} = T_{\infty} + \left(Pr \right)^{\frac{1}{3}} \left(T_{O_{1\infty}} - T_{\infty} \right)$$

from Reference (4). This relationship predicts static temperatures that are much higher than the values calculated from the measured data. A comparison of the actual data to that predicted by Crocco is shown in Figs. 22 and 23 for two different Mach numbers. The experiments would not have shown the inflection point near the surface but the values away from the wall are also much different than the values calculated by Crocco's Relationship. It appears that the Crocco Relationship does not allow for a high enough energy loss to the nozzle wall.

In addition to the above mentioned parameters, the displacement thicknesses and the momentum thicknesses were calculated for each test condition. The displacement thickness is defined as:

$$\frac{\delta^*}{\delta} = \int_0^1 \left(1 - \frac{\rho}{\rho_{\infty}} \frac{V}{V_{\infty}} \right) d \frac{y}{\delta} ,$$

and the momentum thickness is defined as:

$$\frac{\theta}{\delta} = \int_0^1 \frac{\rho}{\rho_{\infty}} \frac{V}{V_{\infty}} \left(1 - \frac{V}{V_{\infty}} \right) d \frac{y}{\delta} .$$

These values along with several other parameters including δ , Re_{θ} , Re_{δ} , Re_{δ^*} , H , and others are listed in Table I.

IV. CONCLUSIONS

A. The pitot pressure and the total temperature profiles were measured across the boundary layer in two hypersonic nozzles at four different conditions each.

B. All of the other parameters across the boundary layer, including δ^* , θ , and H , were calculated for these conditions with the assumption that the static pressure was constant across the boundary layer.

C. A correlation was found to exist between the exponent, n , of the velocity profile power law and the product of the two ratios

$$\frac{T_w}{T_{O_{1\infty}}} \text{ and } \frac{x}{\theta} .$$

D. Crocco's Relationship for the static temperature in terms of the velocity profile predicts temperatures much higher than the calculated value from the measured data except at the wall and the edge of the boundary. These points are forced to match.

E. The velocity profiles exhibit the characteristic shape of turbulent boundary layer profiles shown in Reference (12). Based on this observation, all the boundary layers in this series of tests were assumed to be turbulent.

F. The sonic-pneumatic probe used in this investigation is not considered adequate for examining the flow in the region nearest the wall. It is felt that the results in the outer eighty per cent of the boundary layer are reasonably accurate and this particular probe is a useful tool in this region.

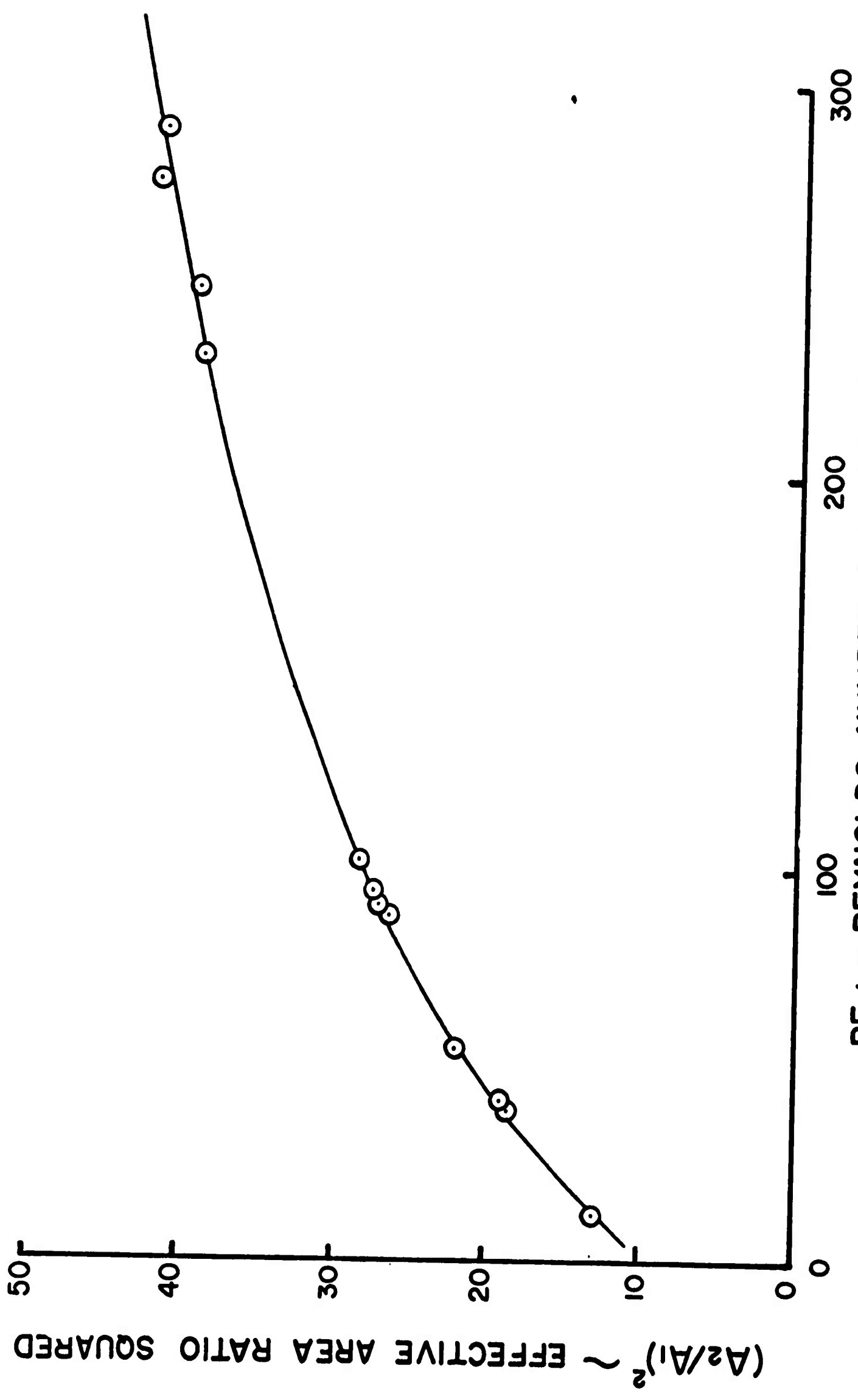
REFERENCES

1. Sichel, Martin, "The Effect of the Boundary Layer Upon the Flow in a Conical Hypersonic Wind Tunnel Nozzle," The University of Michigan, 02953-2-F, July 1963.
2. Lee, John D., "Axisymmetric Nozzles for Hypersonic Flows," Report TN (ALOSU) 459-1, June 1959.
3. Persh, Jerome, "A Theoretical Investigation of Turbulent Boundary Layer Flow with Heat Transfer at Supersonic and Hypersonic Speeds," NAVORD Report 3854, May 1955.
4. Enkenhus, K. R., and Maher, E. F., "The Aerodynamic Design of Axisymmetric Nozzles for High Temperature Air," NAVWEPS Report 7395, February 1962.
5. Sivells, James C. and Payne, Robert G., "A Method of Calculating Turbulent-Boundary-Layer Growth at Hypersonic Mach Numbers," AEDC-TR-59-3, March 1959.
6. Durgin, Frank H., "An Experiment on the Insulating Properties of Boundary Layers," AFOSR TN 57-392, July 1959.
7. Gregorek, G. M., Nark, T. C., and Lee, J. D., "An Experimental Investigation of the Surface Pressure and Laminar Boundary Layer on a Blunt Flat Plate in Hypersonic Flow," Volumes I and II, ASD-TDR-62-792, September 1962.
8. Blackshear, Jr., P. L., "Sonic-Flow Orifice Temperature Probe for High-Gas-Temperature Measurements," NACA TN 2197, September 1950.
9. Thomas, R. E., and Lee, J. D., "The Ohio State University 12-Inch Hypersonic Wind Tunnel System," Report TN (ALOSU) 559-2, July 1959.
10. Welshimer, Don E., "The Experimental Application of Sonic-Pneumatic Probe Systems to Temperature Measurement in a Hypersonic Airstream," ARL 62-364, June 1962.
11. Ames Research Staff, "Equations, Tables and Charts for Compressible Flow," NACA TR 1135, 1953.
12. Schlichting, Dr. Herman, "Boundary Layer Theory," McGraw-Hill Book Company, Inc., New York, New York, 1955.

n	M_∞	Re_x $\times 10^{-6}$	$\frac{T_w}{T_{O_\infty}}$	x (Ft)	T_{O_∞} (°R)	P_{O_∞} (PSIA)	δ (Ft)	$\frac{\delta^*}{\delta}$	$\frac{\theta}{\delta}$
3.31	6.65	0.71	.3118	4.01	1860	42	0.127	.2796	.1240
3.69	11.30	1.18	.2752	4.83	2060	314	0.184	.3730	.0839
4.34	6.46	0.66	.3167	3.51	1860	42	0.108	.2372	.1016
4.85	6.72	2.24	.4082	4.01	1460	95	0.118	.2786	.0958
4.92	11.52	1.28	.2684	5.46	2060	314	0.201	.4489	.0547
6.16	11.40	2.68	.3010	4.83	2060	714	0.151	.3877	.0533
7.17	11.66	2.82	.2913	5.46	2060	714	0.159	.3731	.0477
7.49	6.54	2.05	.4473	3.51	1460	94	0.091	.2435	.0673

n	H	Re_θ $\times 10^{-3}$	Re_{δ^*} $\times 10^{-4}$	Re_δ $\times 10^{-4}$	$\frac{\delta^*}{x}$	$\frac{\delta}{x}$	$\frac{\theta}{x}$	$\frac{D^*}{(Ft)}$
3.31	2.26	2.79	0.62	2.25	.0087	.0317	.0039	.0742
3.69	4.44	3.77	1.68	4.49	.0142	.0371	.0032	.0208
4.34	2.33	2.06	0.48	2.03	.0073	.0307	.0031	.0742
4.85	2.91	6.28	1.83	6.56	.0082	.0293	.0028	.0742
4.92	8.21	2.58	2.11	4.70	.0165	.0367	.0020	.0208
6.16	7.27	4.47	3.25	8.38	.0121	.0313	.0017	.0208
7.17	7.83	3.90	3.06	8.19	.0109	.0291	.0014	.0208
7.49	3.62	3.60	1.30	5.35	.0063	.0261	.0018	.0742

TABLE I
COMPOSITE LISTING OF TEST CONDITIONS
AND
RESULTANT PARAMETERS



RE d ~ REYNOLDS NUMBER AT FIRST THROAT
 FIGURE 2
 CALIBRATION OF SONIC - PNEUMATIC PROBE

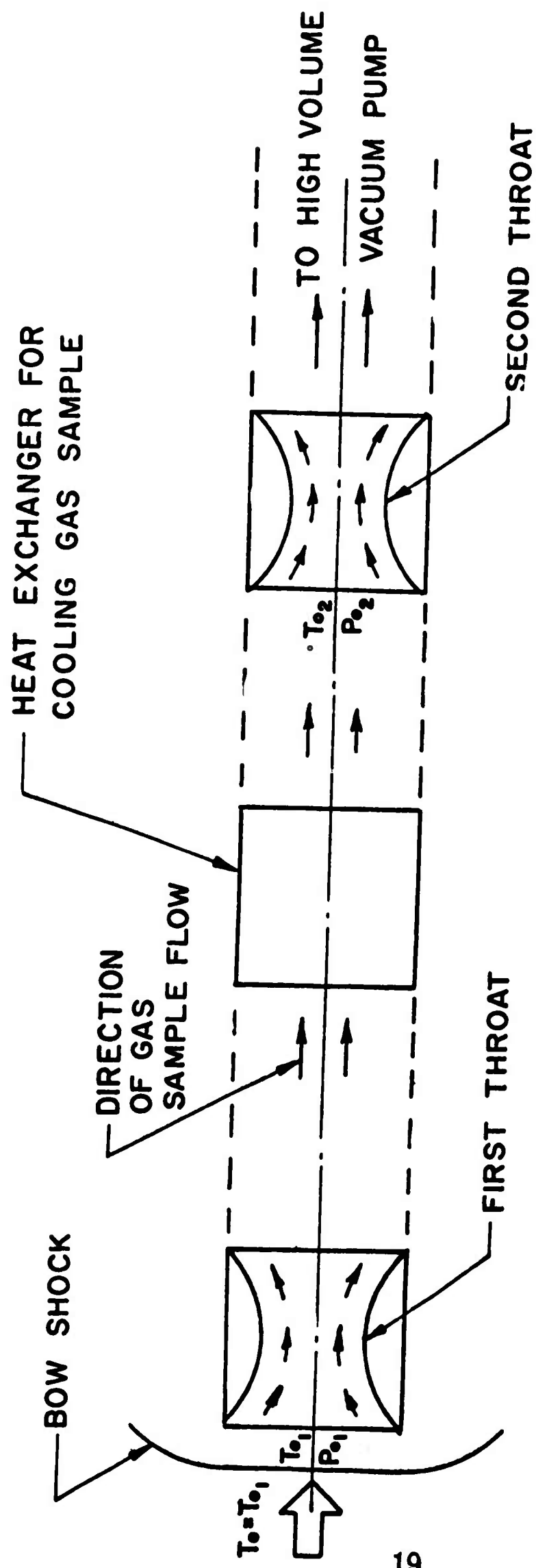


FIGURE 3

SCHEMATIC DIAGRAM OF A SONIC-PNEUMATIC PROBE SYSTEM

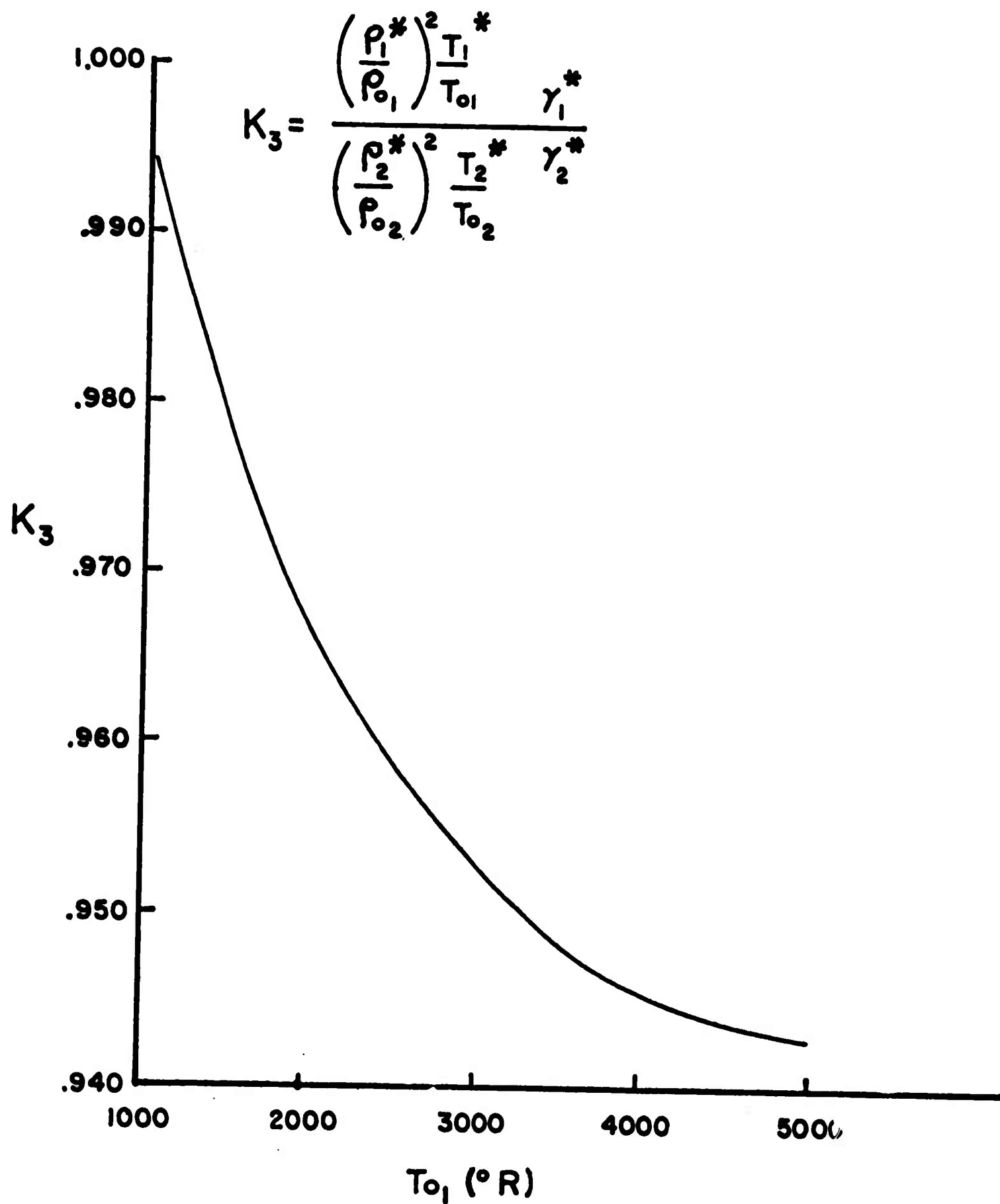
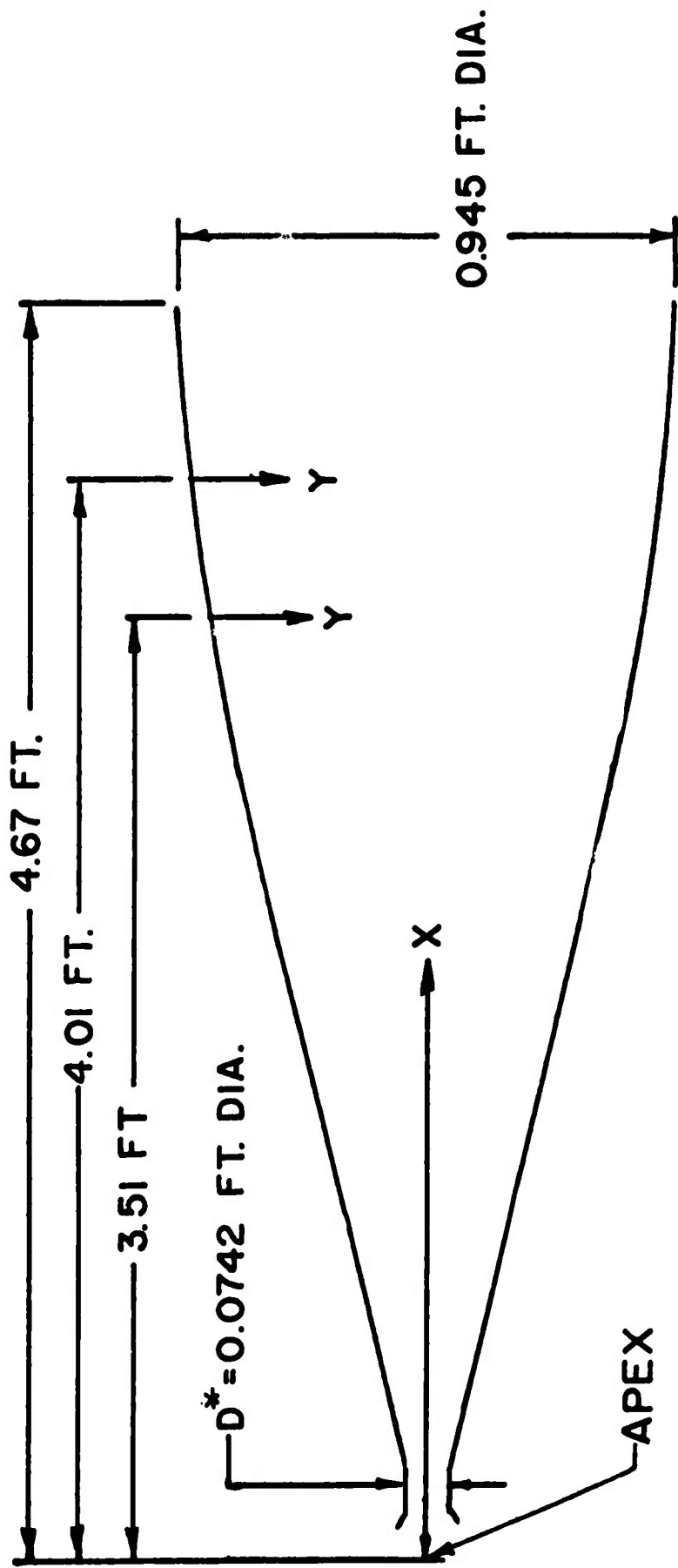
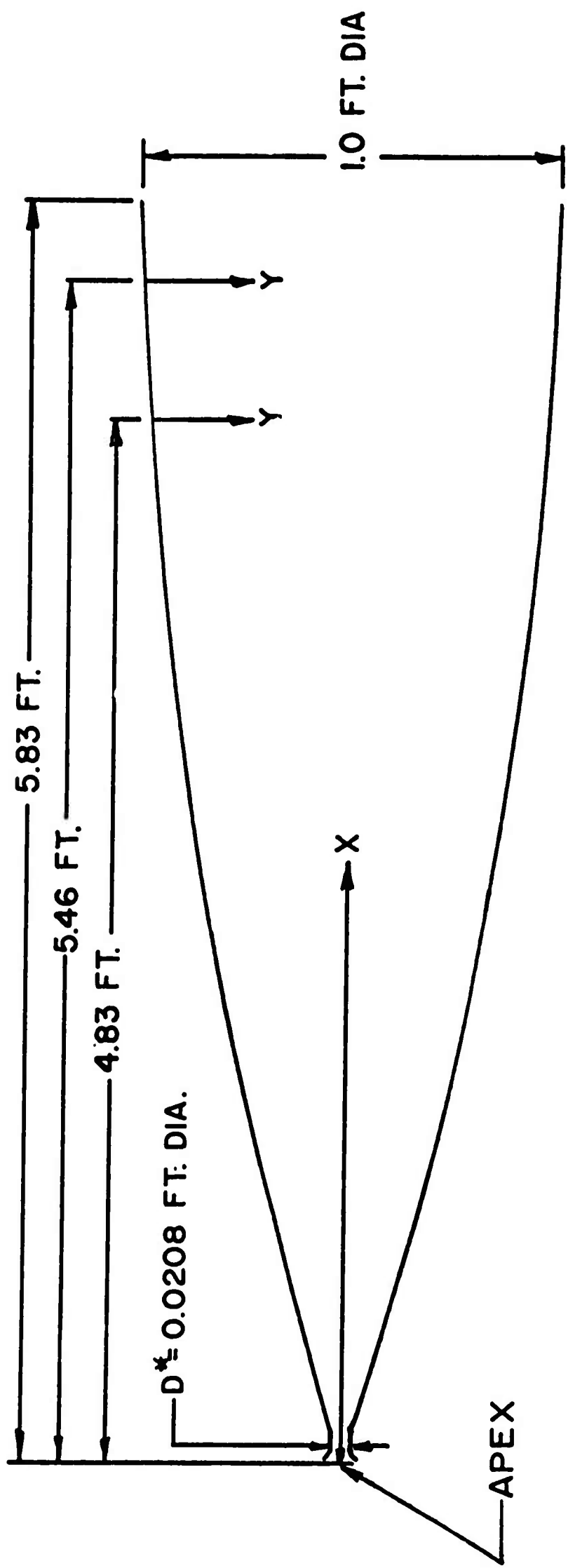


FIGURE 4
CALORIC IMPERFECTION CORRECTION



SCALE = 1" = 10" IN X DIRECTION
 SCALE = 1" = 5" IN Y DIRECTION

FIGURE 5
 MACH SEVEN NOZZLE



SCALE = 1" = 10" IN X DIRECTION
 SCALE = 1" = 5" IN Y DIRECTION

FIGURE 6
 MACH TWELVE NOZZLE

○ $M_\infty = 6.65$, $Re_x = 0.71 \times 10^6$, $T_w/T_{o,1\infty} = 0.3118$
 $\delta = 0.127$ FT.

□ $M_\infty = 6.72$, $Re_x = 2.24 \times 10^6$, $T_w/T_{o,1\infty} = 0.4082$
 $\delta = 0.118$ FT.

△ $M_\infty = 6.46$, $Re_x = 0.66 \times 10^6$, $T_w/T_{o,1\infty} = 0.3167$
 $\delta = 0.108$ FT.

▴ $M_\infty = 6.54$, $Re_x = 2.05 \times 10^6$, $T_w/T_{o,1\infty} = 0.4473$
 $\delta = 0.091$ FT.

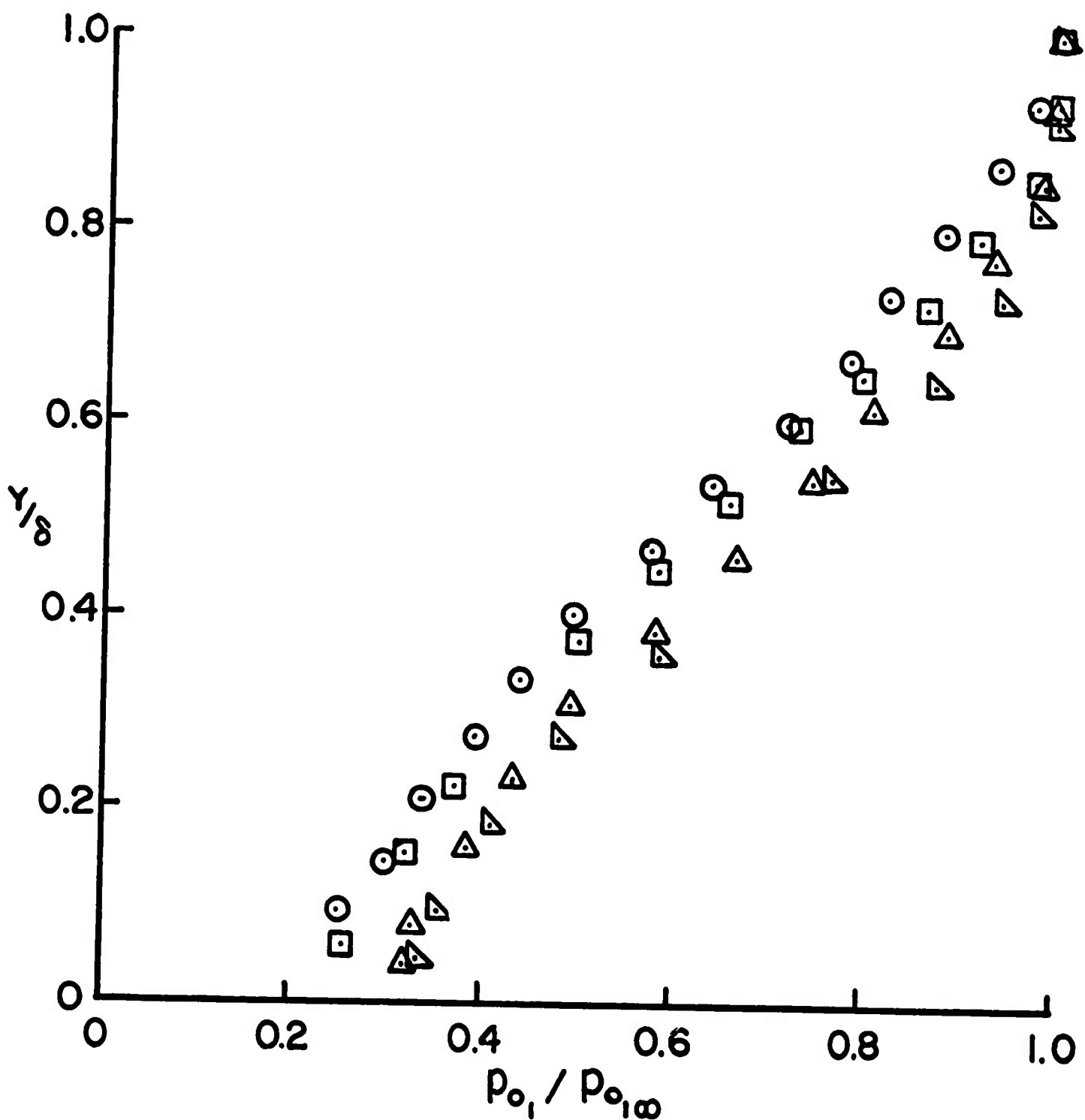


FIGURE 7

PITOT PRESSURE PROFILES AT MACH 6.5

□ $M_\infty = 11.52$, $Re_x = 1.28 \times 10^6$, $T_w/T_{o,\infty} = 0.2684$
 $\delta = 0.201$ FT.

△ $M_\infty = 11.30$, $Re_x = 1.18 \times 10^6$, $T_w/T_{o,\infty} = 0.2752$
 $\delta = 0.184$ FT.

○ $M_\infty = 11.66$, $Re_x = 2.82 \times 10^6$, $T_w/T_{o,\infty} = 0.2913$
 $\delta = 0.159$ FT.

▴ $M_\infty = 11.40$, $Re_x = 2.68 \times 10^6$, $T_w/T_{o,\infty} = 0.3010$
 $\delta = 0.151$ FT.

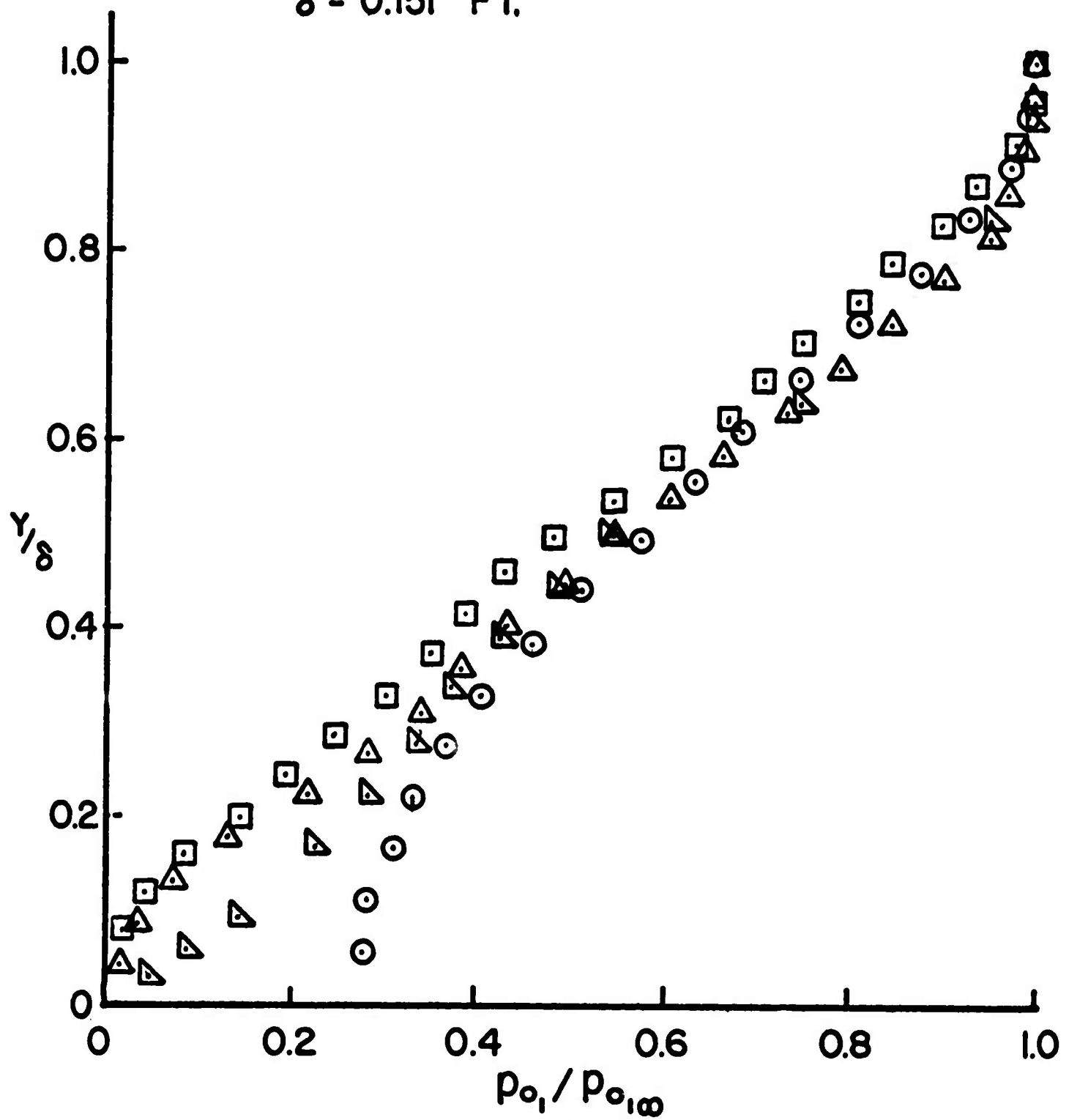


FIGURE 8

PITOT PRESSURE PROFILES AT MACH 11.5

- $\odot M_{\infty} = 6.65, Re_x = 0.71 \times 10^6, Tw/T_{o,\infty} = 0.3118$
 $\triangle M_{\infty} = 6.72, Re_x = 2.24 \times 10^6, Tw/T_{o,\infty} = 0.4082$
 $\square M_{\infty} = 6.46, Re_x = 0.66 \times 10^6, Tw/T_{o,\infty} = 0.3167$
 $\nabla M_{\infty} = 6.54, Re_x = 2.06 \times 10^6, Tw/T_{o,\infty} = 0.4473$

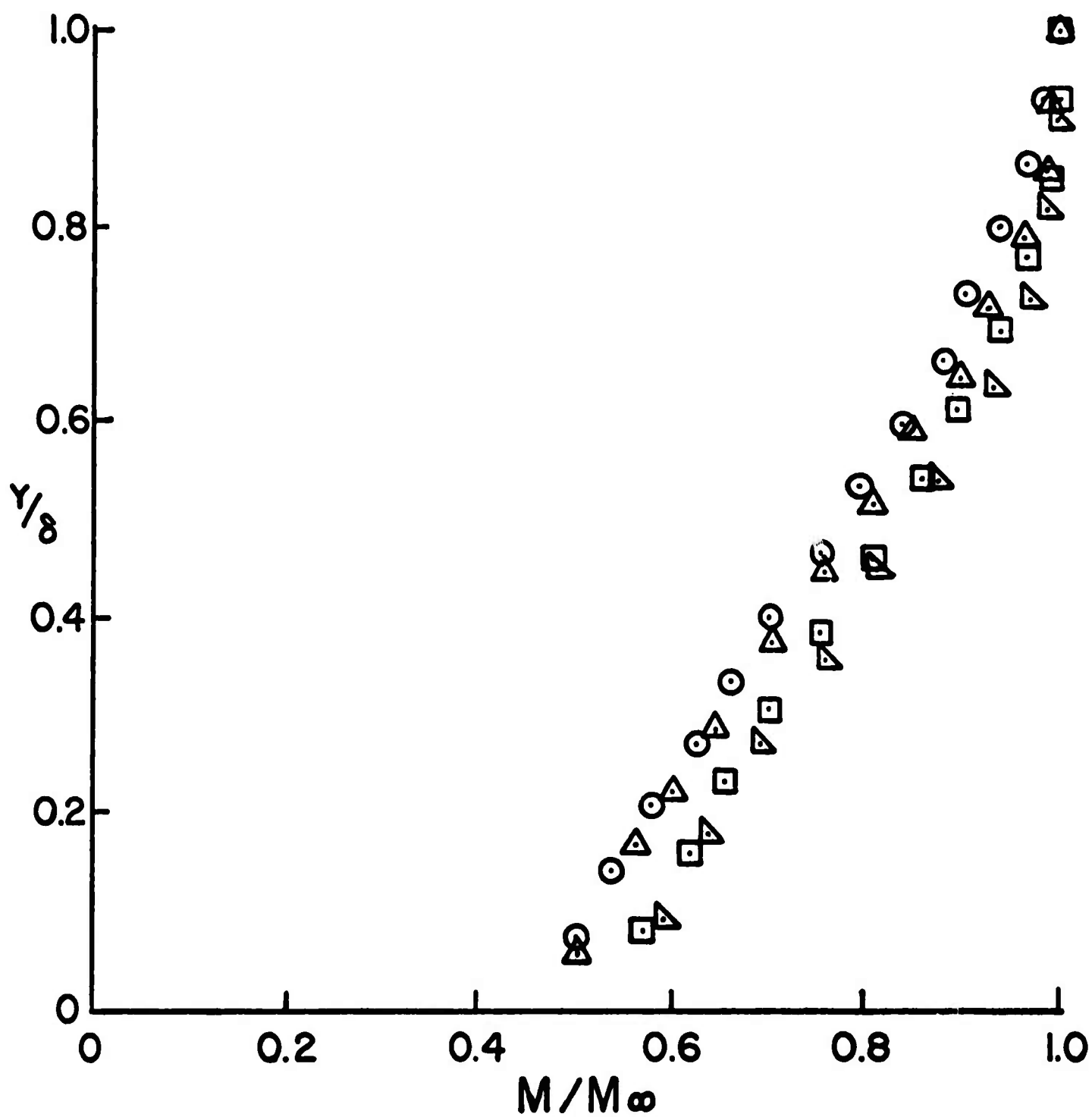


FIGURE 9

MACH NUMBER PROFILES AT MACH 6.5

○ $M_\infty = 11.66$, $Re_x = 2.82 \times 10^6$, $T_w/T_{o,\infty} = 0.2913$

△ $M_\infty = 11.52$, $Re_x = 1.28 \times 10^6$, $T_w/T_{o,\infty} = 0.2684$

□ $M_\infty = 11.30$, $Re_x = 1.18 \times 10^6$, $T_w/T_{o,\infty} = 0.2752$

▴ $M_\infty = 11.40$, $Re_x = 2.68 \times 10^6$, $T_w/T_{o,\infty} = 0.3010$

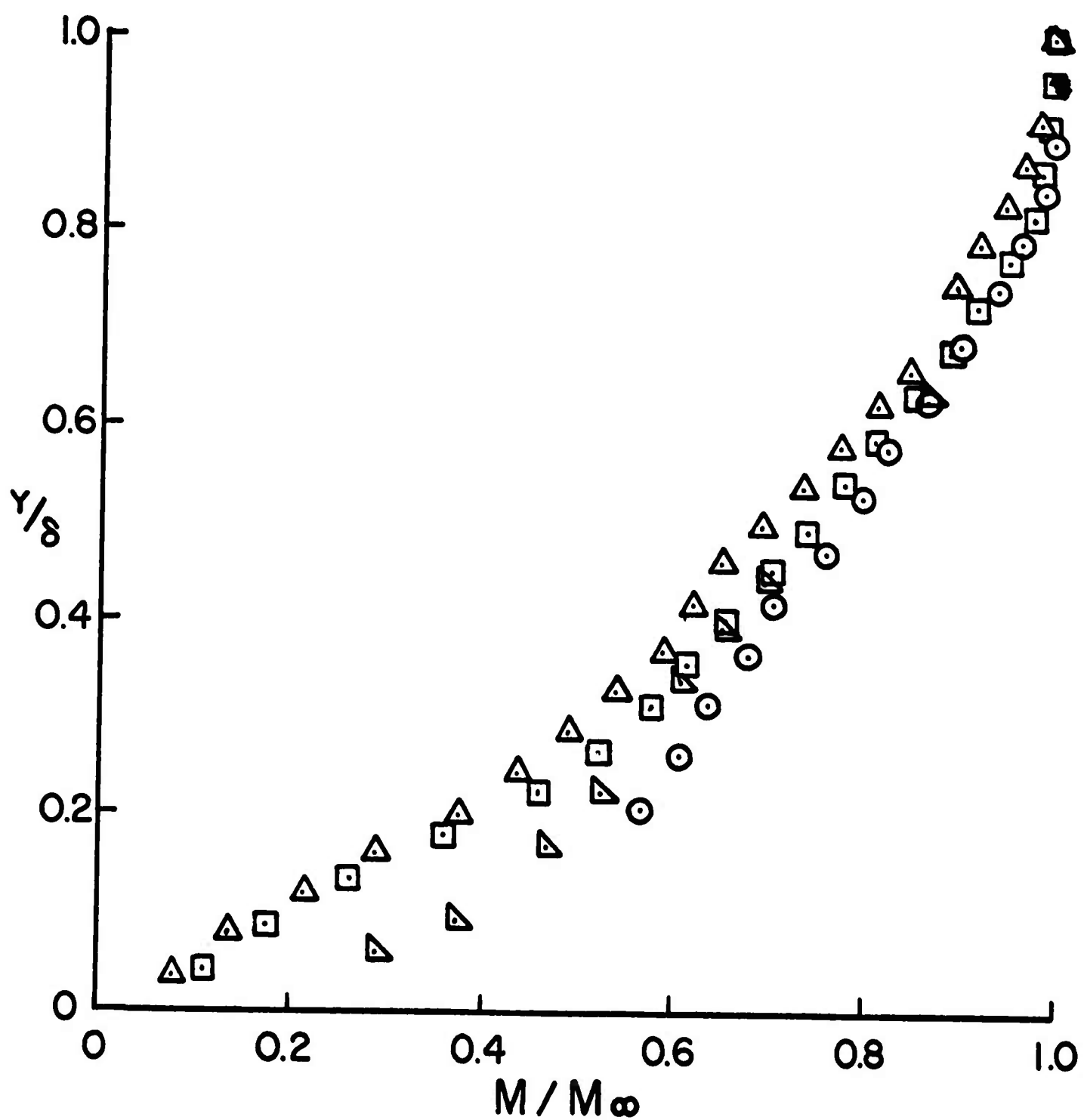


FIGURE 10

MACH NUMBER PROFILES AT MACH 11.5

- \odot $M_\infty = 6.65$, $Re_x = 0.71 \times 10^6$, $T_w / T_{o, \infty} = 0.3118$
 $\delta = 0.127$ FT.
 \triangleleft $M_\infty = 6.46$, $Re_x = 0.61 \times 10^6$, $T_w / T_{o, \infty} = 0.3167$
 $\delta = 0.1080$ FT.
 \square $M_\infty = 6.72$, $Re_x = 2.24 \times 10^6$, $T_w / T_{o, \infty} = 0.4082$
 $\delta = 0.1167$ FT.
 \triangle $M_\infty = 6.54$, $Re_x = 2.05 \times 10^6$, $T_w / T_{o, \infty} = 0.4473$
 $\delta = 0.0914$ FT.

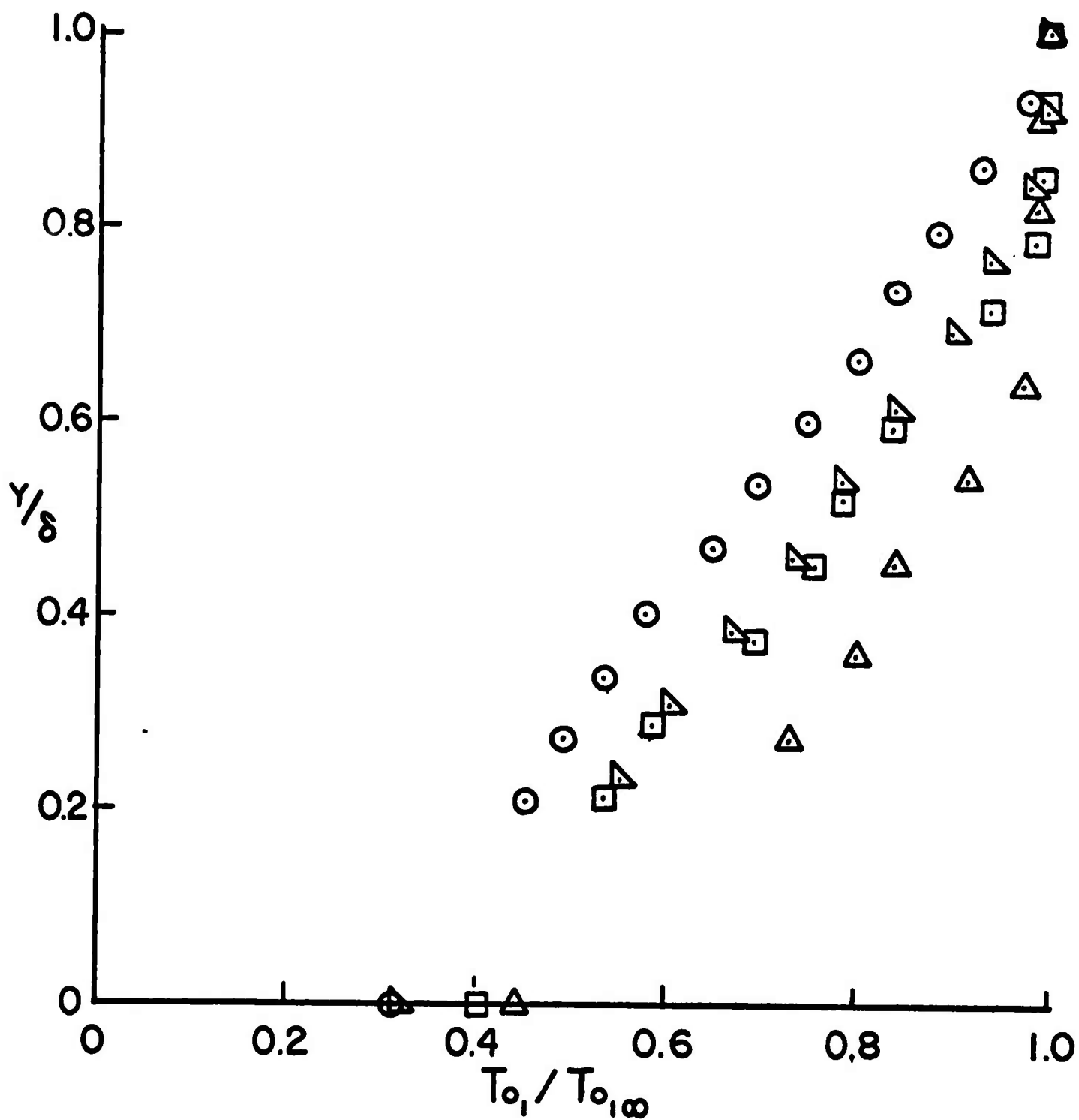


FIGURE 11

TOTAL TEMPERATURE PROFILES AT MACH 6.5

- \triangle $M_\infty = 11.30$, $Re_x = 1.18 \times 10^6$, $T_w/T_{o, \infty} = 0.2752$
 $\delta = 0.184$ FT.
 \square $M_\infty = 11.52$, $Re_x = 1.28 \times 10^6$, $T_w/T_{o, \infty} = 0.2684$
 $\delta = 0.201$ FT.
 \triangleleft $M_\infty = 11.40$, $Re_x = 2.68 \times 10^6$, $T_w/T_{o, \infty} = 0.3010$
 $\delta = 0.151$ FT.
 \odot $M_\infty = 11.66$, $Re_x = 2.82 \times 10^6$, $T_w/T_{o, \infty} = 0.2913$
 $\delta = 0.159$ FT.

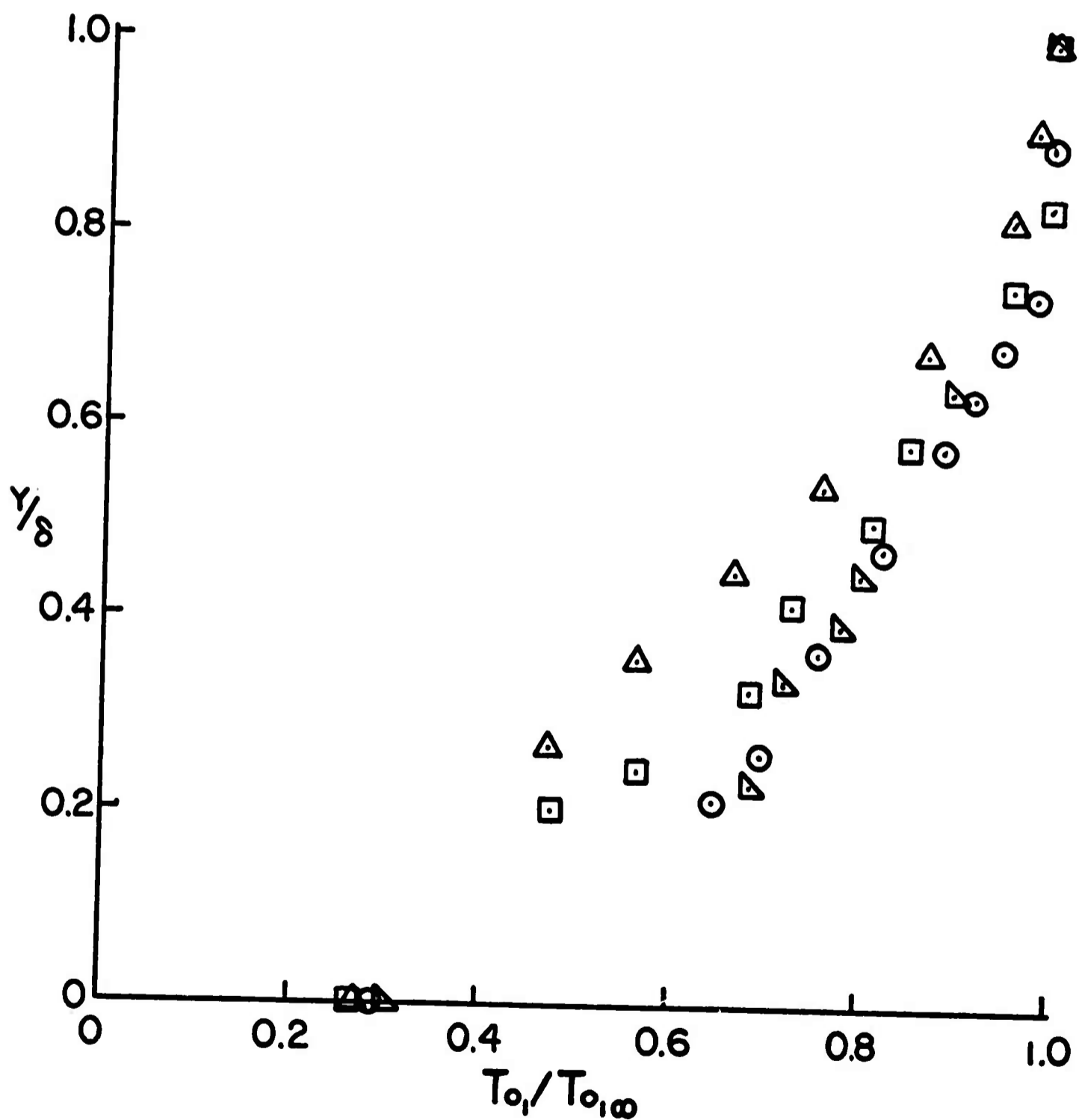


FIGURE 12

TOTAL TEMPERATURE PROFILES AT MACH 11.5

$\odot V / V_{\infty}$
 $\triangle M / M_{\infty}$
 $\square T / T_{o, \infty}$
 $\text{—} (Y/\delta)^{1/3.31}$

$M_{\infty} = 6.65$, $Re_x = 0.71 \times 10^6$, $T_w / T_{o, \infty} = 0.3118$
 $T_{o, \infty} = 1860^{\circ}R$, $P_{o, \infty} = 42 \text{ PSIA}$, $P_{\infty} = 0.0134 \text{ PSIA}$
 $T_{\infty} = 186^{\circ}R$, $\delta = 0.127 \text{ FT.}$, $\delta^* / \delta = 0.2796$
 $\theta / \delta = 0.1240$, $H = 2.26$, $X = 4.01 \text{ FT.}$

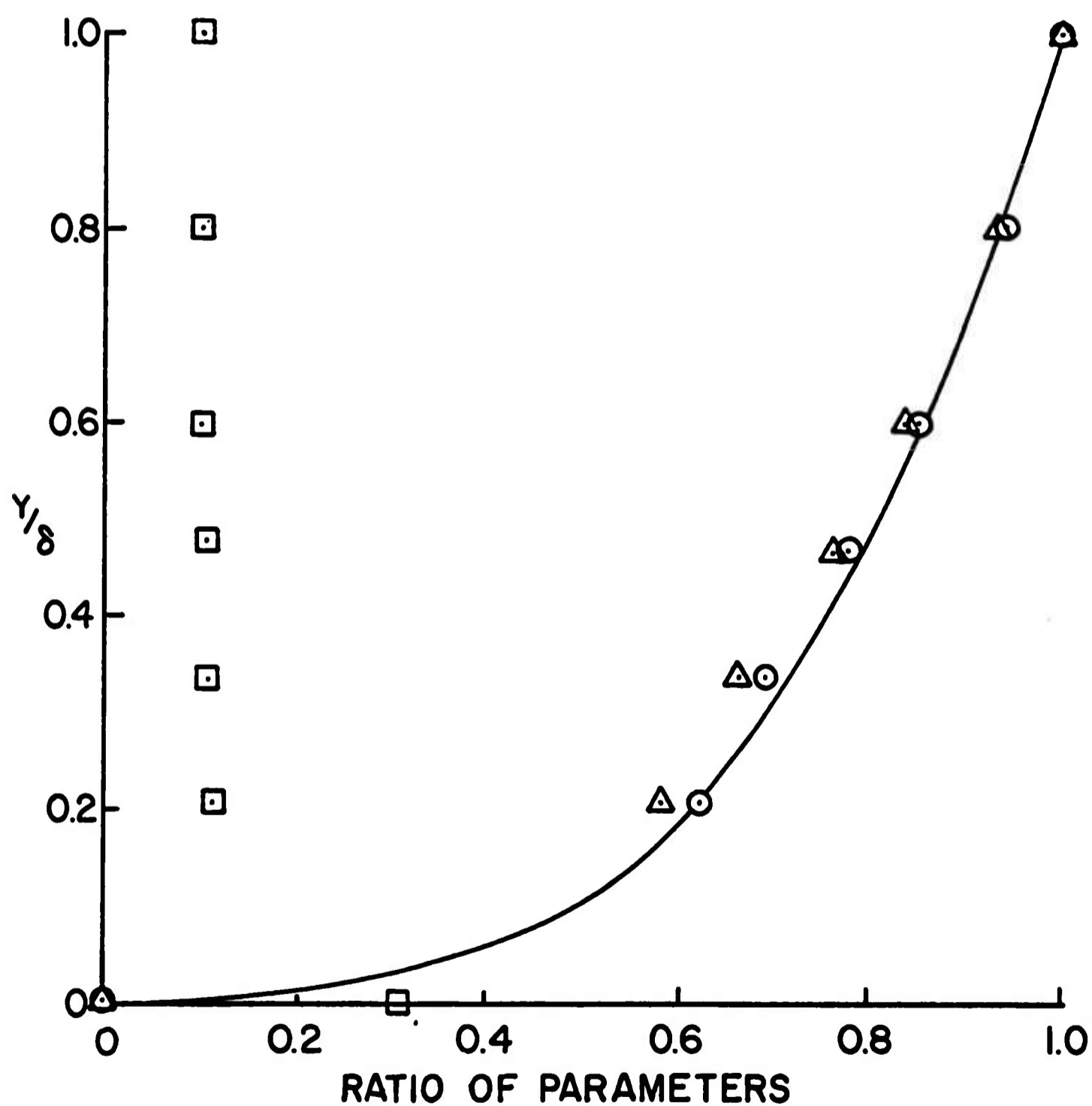


FIGURE 13

MACH NUMBER, VELOCITY, AND STATIC TEMP. PROFILES

$\odot V/V_\infty$
 $\triangle M/M_\infty$
 $\square T/T_{o,\infty}$
 $\text{---} (Y/\delta)^{1/4.34}$

$M_\infty = 6.46$, $Re_x = 0.66 \times 10^6$, $T_w/T_{o,\infty} = 0.3167$
 $T_{o,\infty} = 1860^\circ R$, $P_{o,\infty} = 42 \text{ PSIA}$, $P_\infty = 0.0161 \text{ PSIA}$
 $T_\infty = 199^\circ R$, $\delta = 0.1080 \text{ FT.}$, $\delta^*/\delta = 0.2372$
 $\theta/\delta = 0.1016$, $H = 2.33$, $X = 3.51 \text{ FT.}$

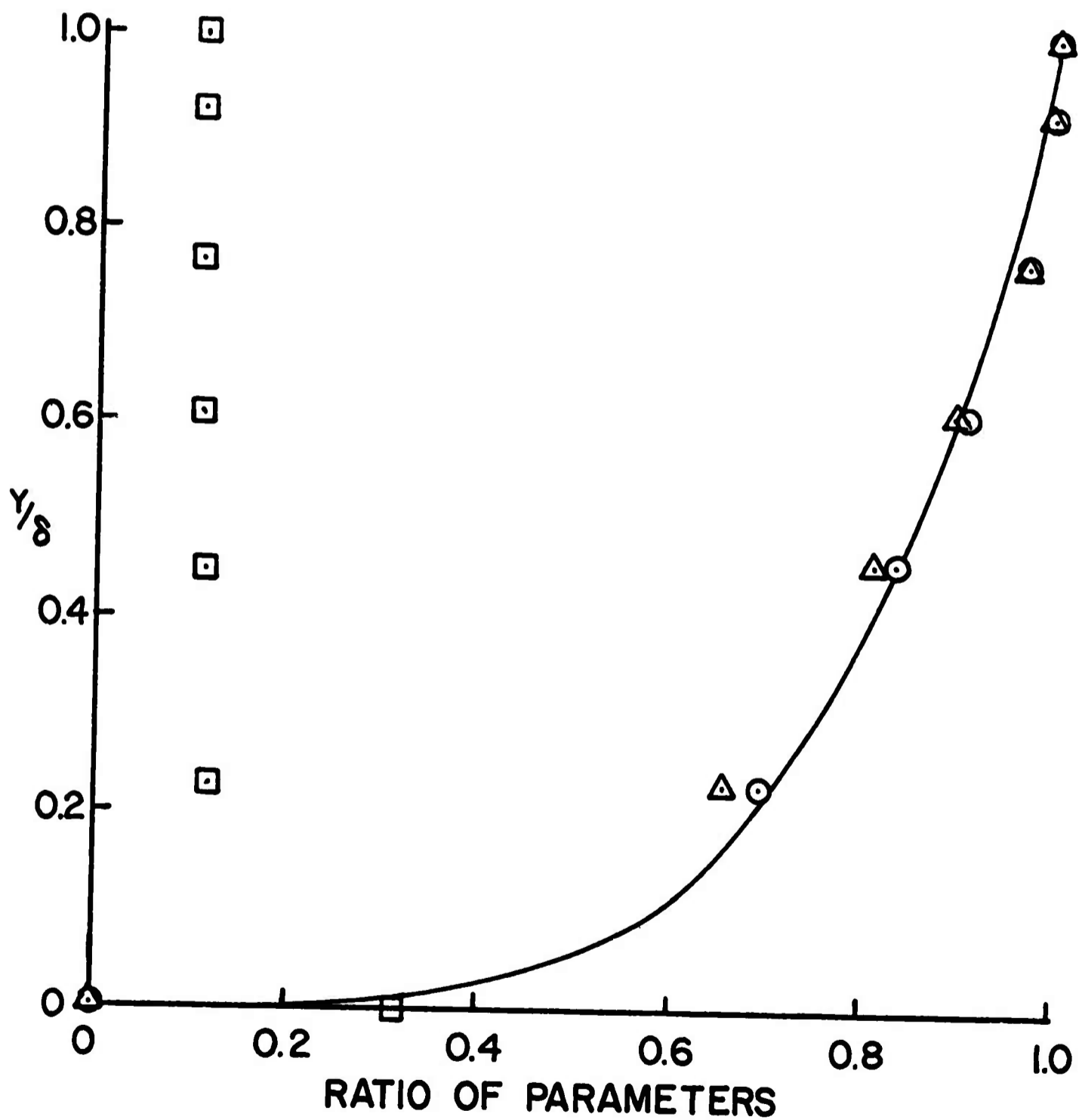


FIGURE 14
 MACH NUMBER, VELOCITY, AND STATIC TEMP. PROFILES

$\odot V/V_\infty$
 $\triangle M/M_\infty$
 $\square T/T_{o,1\infty}$
 $\text{---} (Y/\delta)^{1/4.85}$

$M_\infty = 6.72$, $Re_x = 2.24 \times 10^6$, $T_w/T_{o,1\infty} = 0.4082$
 $T_{o,1\infty} = 1460^\circ R$, $p_{o,\infty} = 95 \text{ PSIA}$, $p_\infty = 0.0291 \text{ PSIA}$
 $T_\infty = 145^\circ R$, $\delta = 0.1176 \text{ FT.}$, $\delta^*/\delta = 0.2786$
 $\theta/\delta = 0.0958$, $H = 2.91$, $X = 4.01 \text{ FT.}$

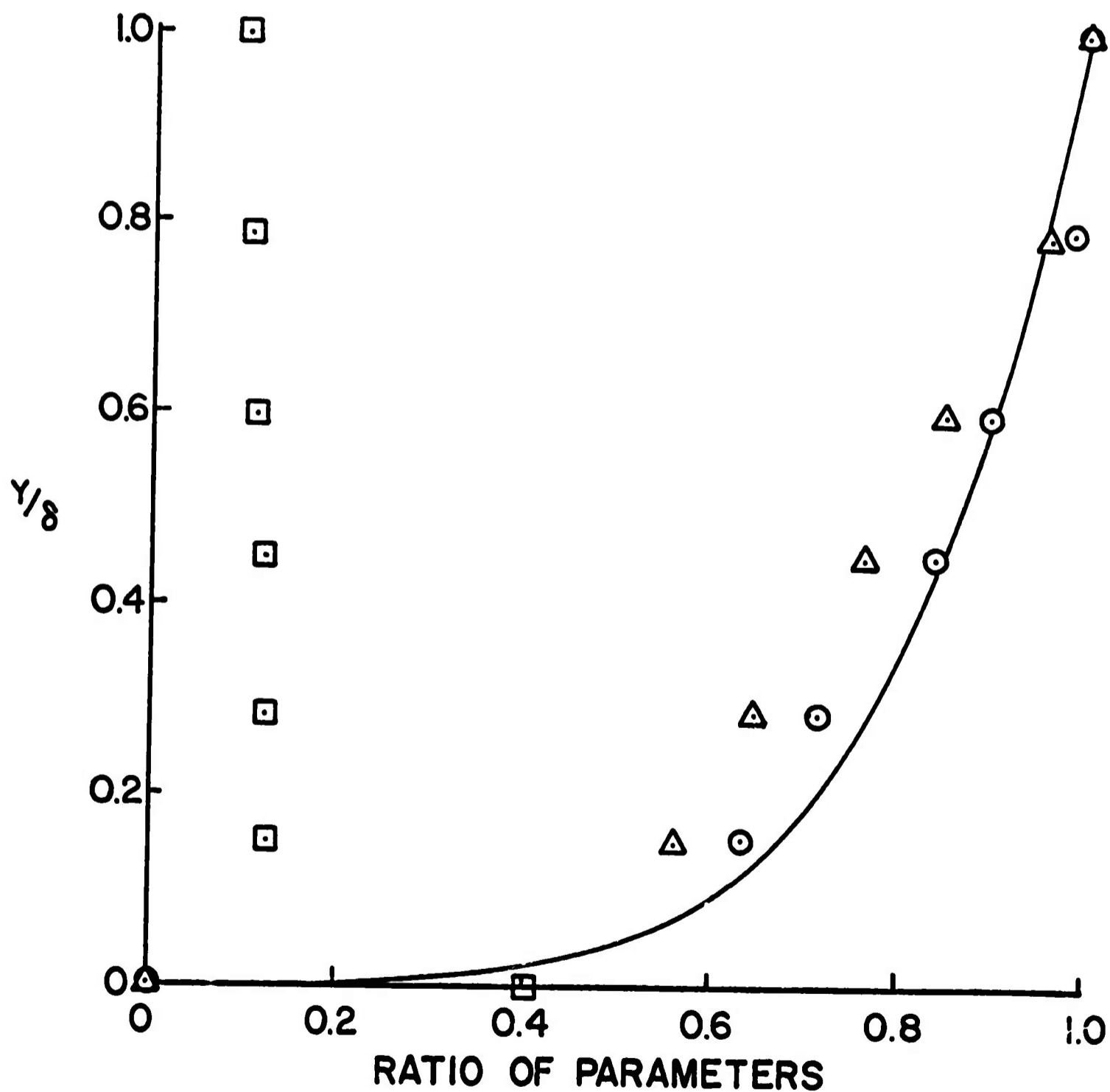


FIGURE 15

MACH NUMBER, VELOCITY, AND STATIC TEMP. PROFILES

\odot V/V_∞
 \triangle M/M_∞
 \square $T/T_{01\infty}$
 — $(Y/\delta)^{1/7.49}$

$M_\infty = 6.54$, $Re_x = 2.05 \times 10^6$, $T_w/T_{01\infty} = 0.4473$
 $T_{01\infty} = 1460^\circ R$, $P_{0\infty} = 94 \text{ PSIA}$, $P_\infty = 0.0341 \text{ PSIA}$
 $T_\infty = 153^\circ R$, $\delta = 0.0914 \text{ FT.}$, $\delta^*/\delta = 0.2435$
 $\theta/\delta = 0.0673$, $H = 3.62$, $X = 3.51 \text{ FT.}$

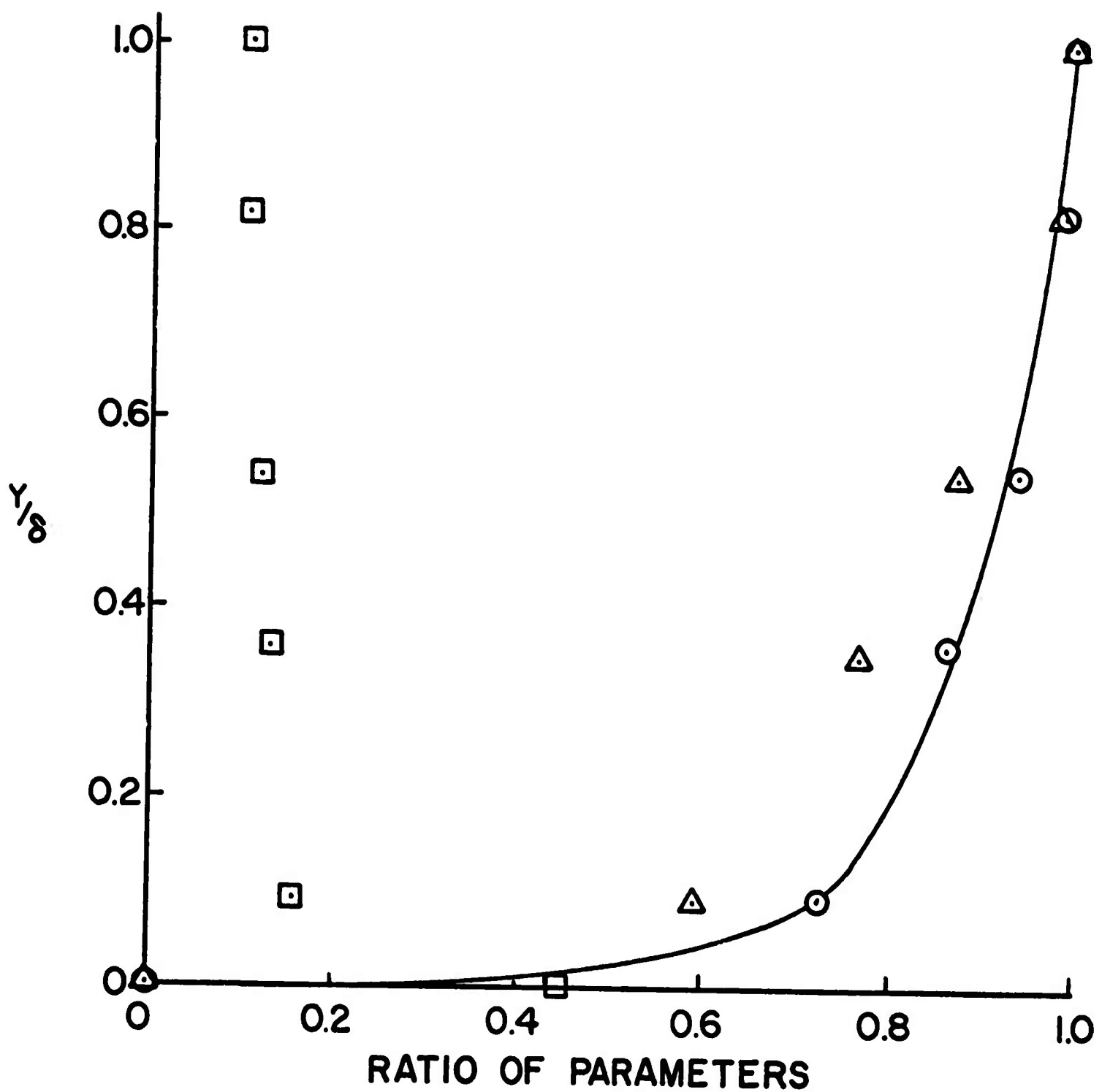


FIGURE 16

MACH NUMBER, VELOCITY, AND STATIC TEMP. PROFILES

$\odot V/V_\infty$
 $\triangle M/M_\infty$
 $\square T/T_{o1\infty}$
 $\text{---} (Y/\delta)^{1/3.69}$

$M_\infty = 11.30, Re_x = 1.18 \times 10^6, T_w/T_{o1\infty} = 0.2752$
 $T_{o1\infty} = 2060^\circ R, \rho_{o\infty} = 314 \text{ PSIA}, \rho_\infty = 0.0031 \text{ PSIA}$
 $T_\infty = 78^\circ R, \delta = 0.1842 \text{ FT.}, \delta^*/\delta = 0.3730$
 $\theta/\delta = 0.0839, H = 4.44, X = 4.83 \text{ FT.}$

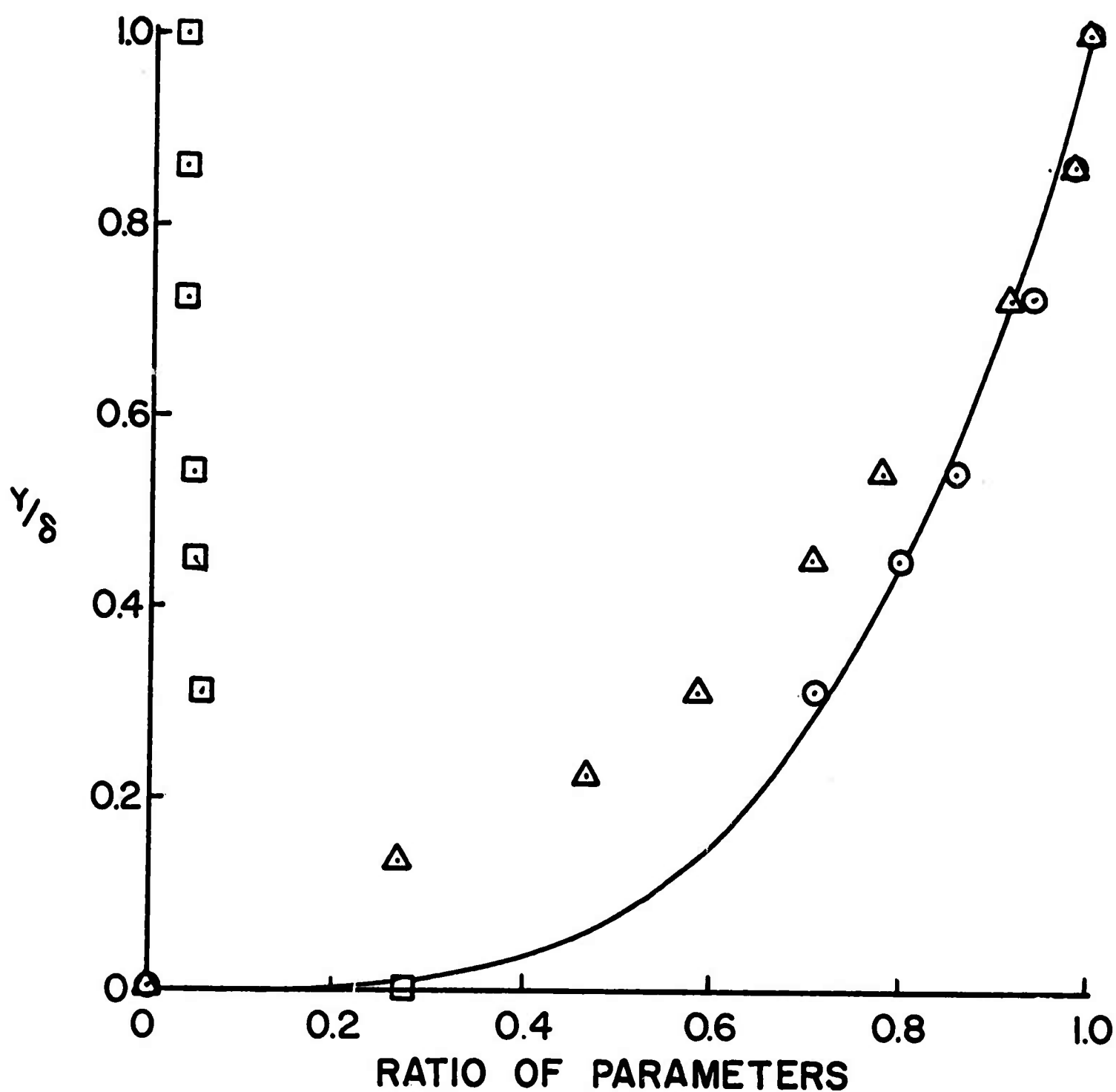


FIGURE 17

MACH NUMBER, VELOCITY, AND STATIC TEMP. PROFILES

\odot V/V_∞
 \triangle M/M_∞
 \square $T/T_{o,1\infty}$
 — $(Y/\delta)^{1/4.92}$

$M_\infty = 11.52$, $Re_x = 1.28 \times 10^6$, $T_w/T_{o,1\infty} = 0.2684$
 $T_{o,1\infty} = 2060^\circ R$, $P_{o,1\infty} = 314$ PSIA, $P_\infty = 0.0027$ PSIA
 $T_\infty = 75^\circ R$, $\delta = 0.2010$ FT., $\delta^*/\delta = 0.4489$
 $\theta/\delta = 0.0547$, $H = 8.21$, $X = 5.46$ FT.

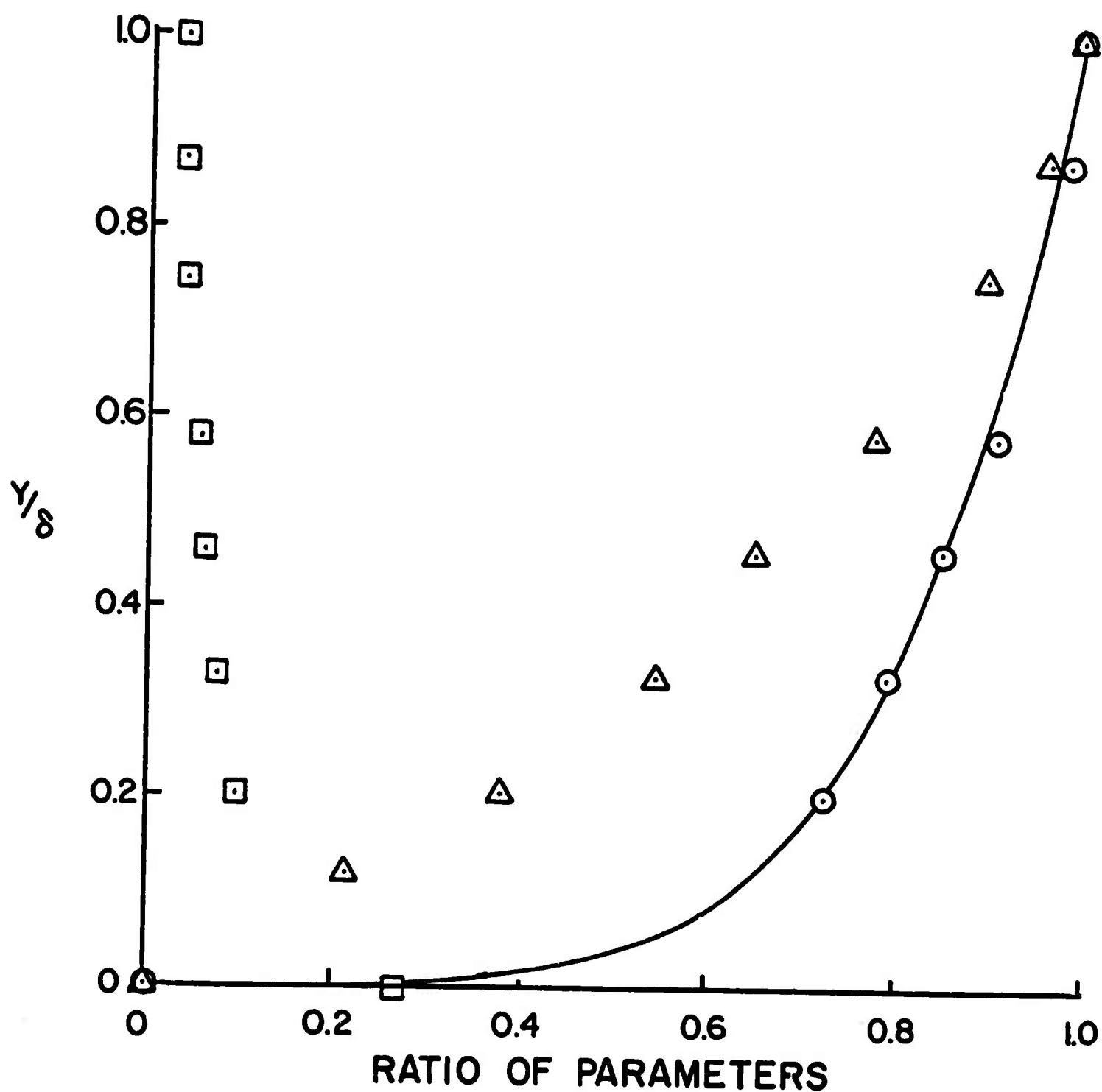


FIGURE 18

MACH NUMBER, VELOCITY, AND STATIC TEMP. PROFILES

$\odot V/V_\infty$
 $\triangle M/M_\infty$
 $\square T/T_{o,\infty}$
 $\text{---} (Y/\delta)^{1/6.16}$

$M_\infty = 11.40$, $Re_x = 2.68 \times 10^6$, $T_w/T_{o,\infty} = 0.3010$
 $T_{o,\infty} = 2060^\circ R$, $P_{o,\infty} = 714 \text{ PSIA}$, $P_\infty = 0.0065 \text{ PSIA}$
 $T_\infty = 76^\circ R$, $\delta = 0.1512 \text{ FT.}$, $\delta^*/\delta = 0.3877$
 $\theta/\delta = 0.0533$, $H = 7.27 \text{ FT.}$, $X = 4.83 \text{ FT.}$

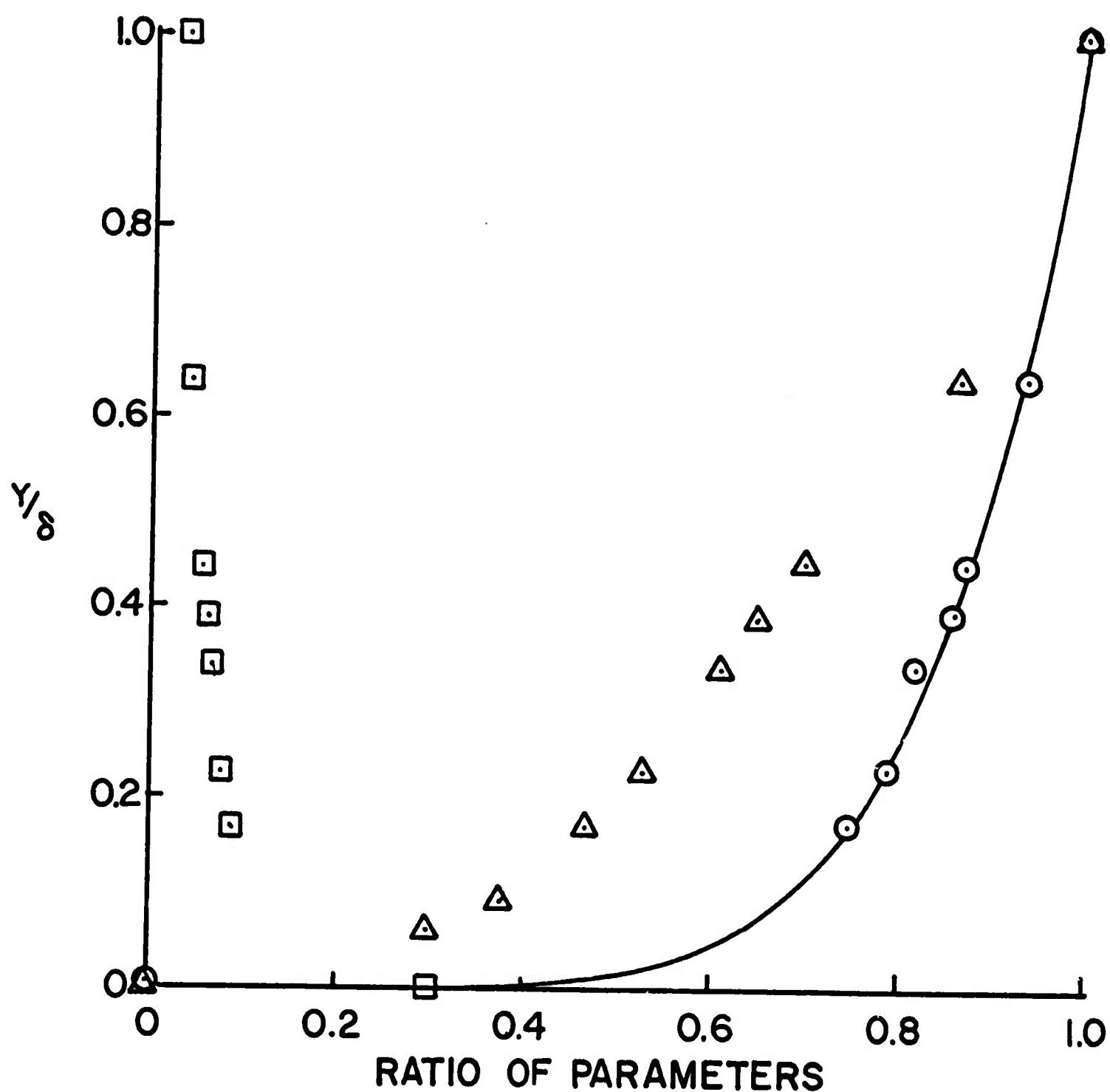


FIGURE 19

MACH NUMBER, VELOCITY, AND STATIC TEMP. PROFILES

$\odot V/V_\infty$
 $\triangle M/M_\infty$
 $\square T/T_{o1\infty}$
 $\text{—} (Y/\delta)^{1/7.17}$

$M_\infty = 11.66$, $Re_x = 2.82 \times 10^6$, $T_w/T_{o1\infty} = 0.2913$
 $T_{o1\infty} = 2060^\circ R$, $P_{o\infty} = 714 \text{ PSIA}$, $P_\infty = 0.0056 \text{ PSIA}$
 $T_\infty = 73^\circ R$, $\delta = 0.1587 \text{ FT.}$, $\delta^*/\delta = 0.3731$
 $\theta/\delta = 0.0477$, $H = 7.83$, $X = 5.46 \text{ FT.}$

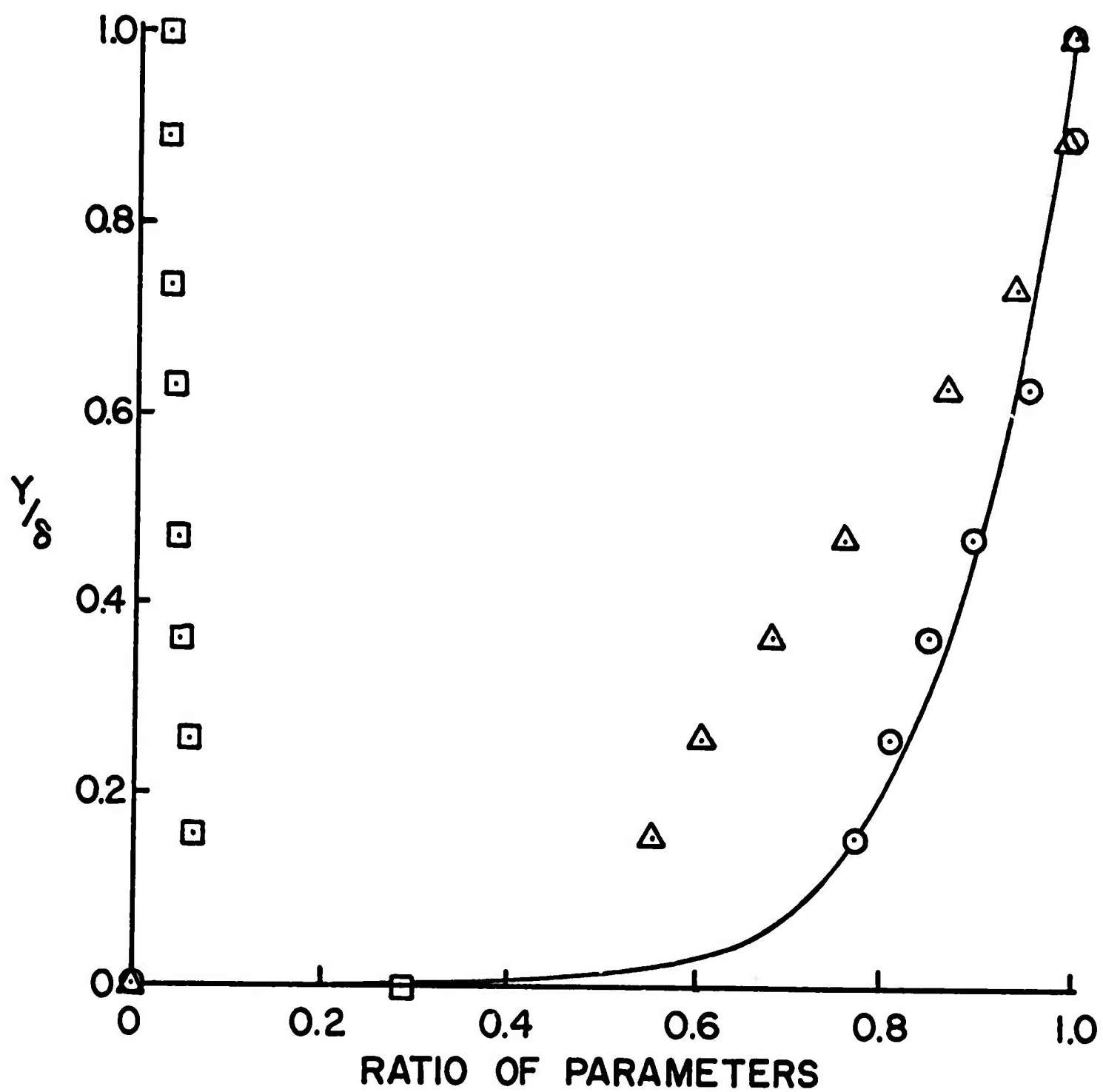


FIGURE 20

MACH NUMBER, VELOCITY, AND STATIC TEMP. PROFILES

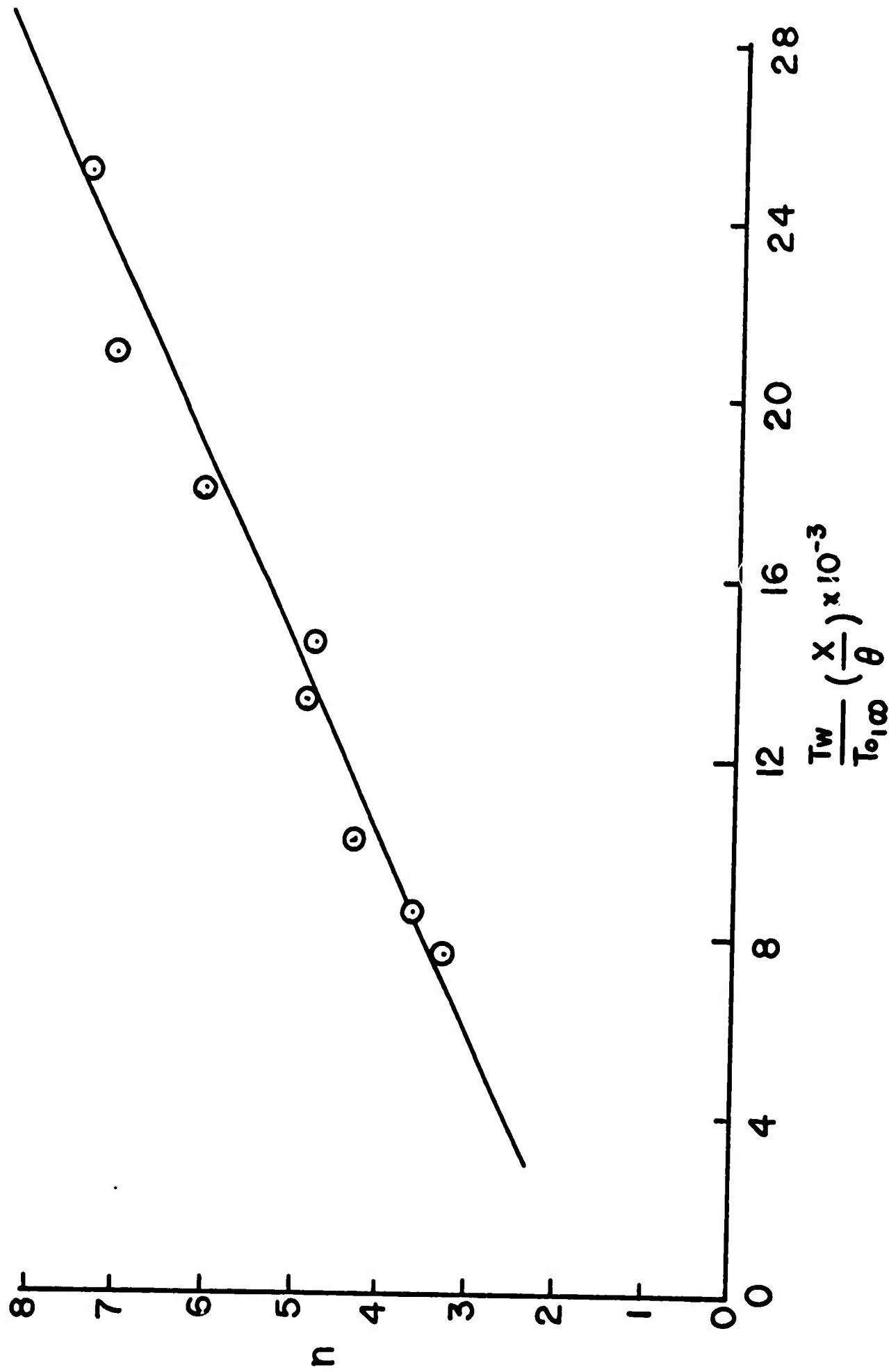


FIGURE 21

CORRELATION OF VELOCITY PROFILE POWER LAW EXPONENT

$$\delta = 0.108 \text{ FT.}$$

REFERENCE (4)

$$T/T_{0,\infty} = 0.3167 + 0.5863 V/V_\infty - 0.7960 (V/V_\infty)^2$$

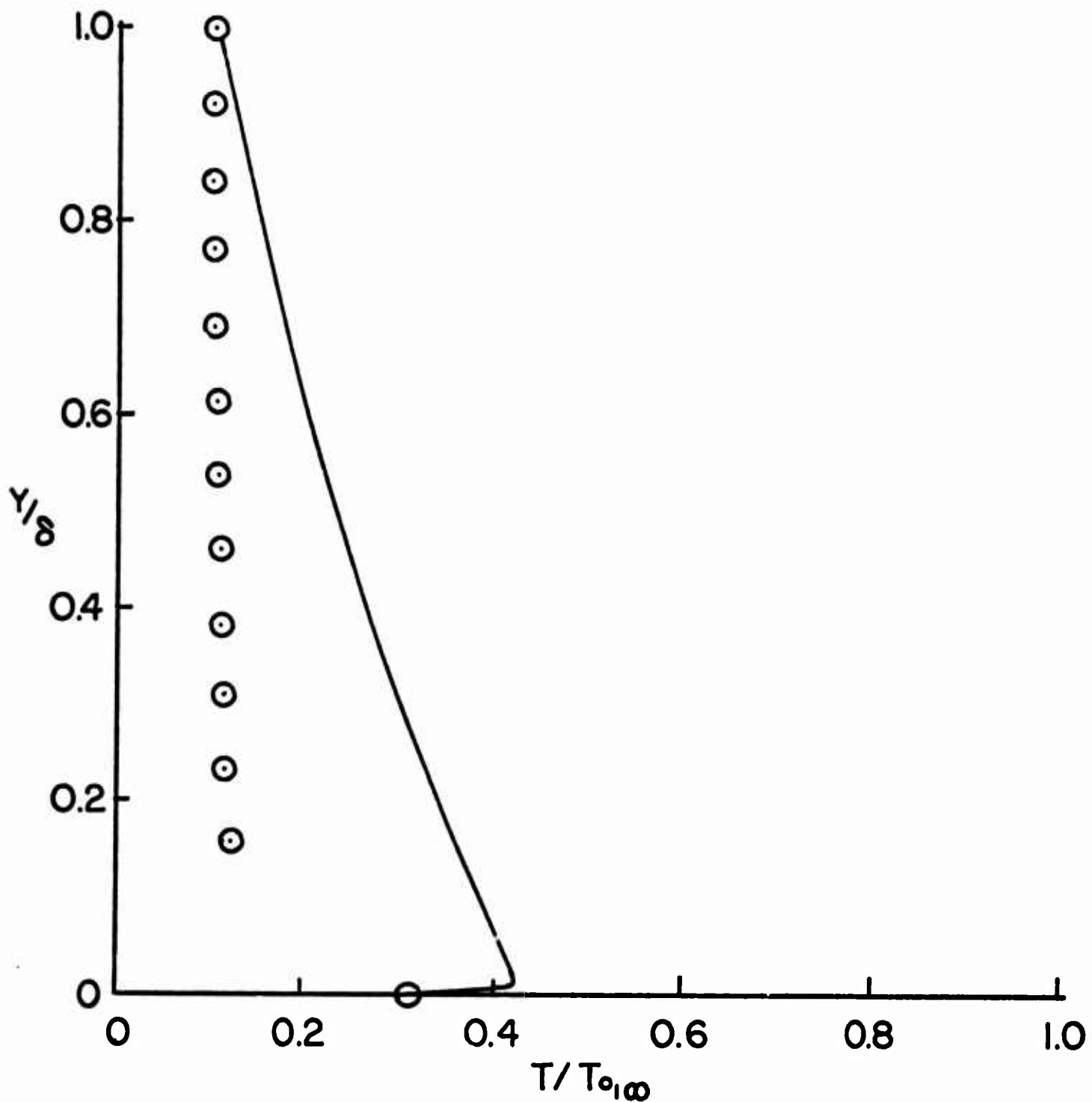


FIGURE 22
COMPARISON OF STATIC TEMP. PROFILE
AT MACH 6.5

○ $M_\infty = 11.66$, $Re_x = 2.82 \times 10^6$, $T_w/T_{o_{1\infty}} = 0.2913$
 $\delta = 0.159$ FT.

— CALCULATED FROM CROCCO'S RELATIONSHIP
 REFERENCE (4)

$$T/T_{o_{1\infty}} = 0.2913 + 0.6087 V/V_\infty - 0.8660 (V/V_\infty)^2$$

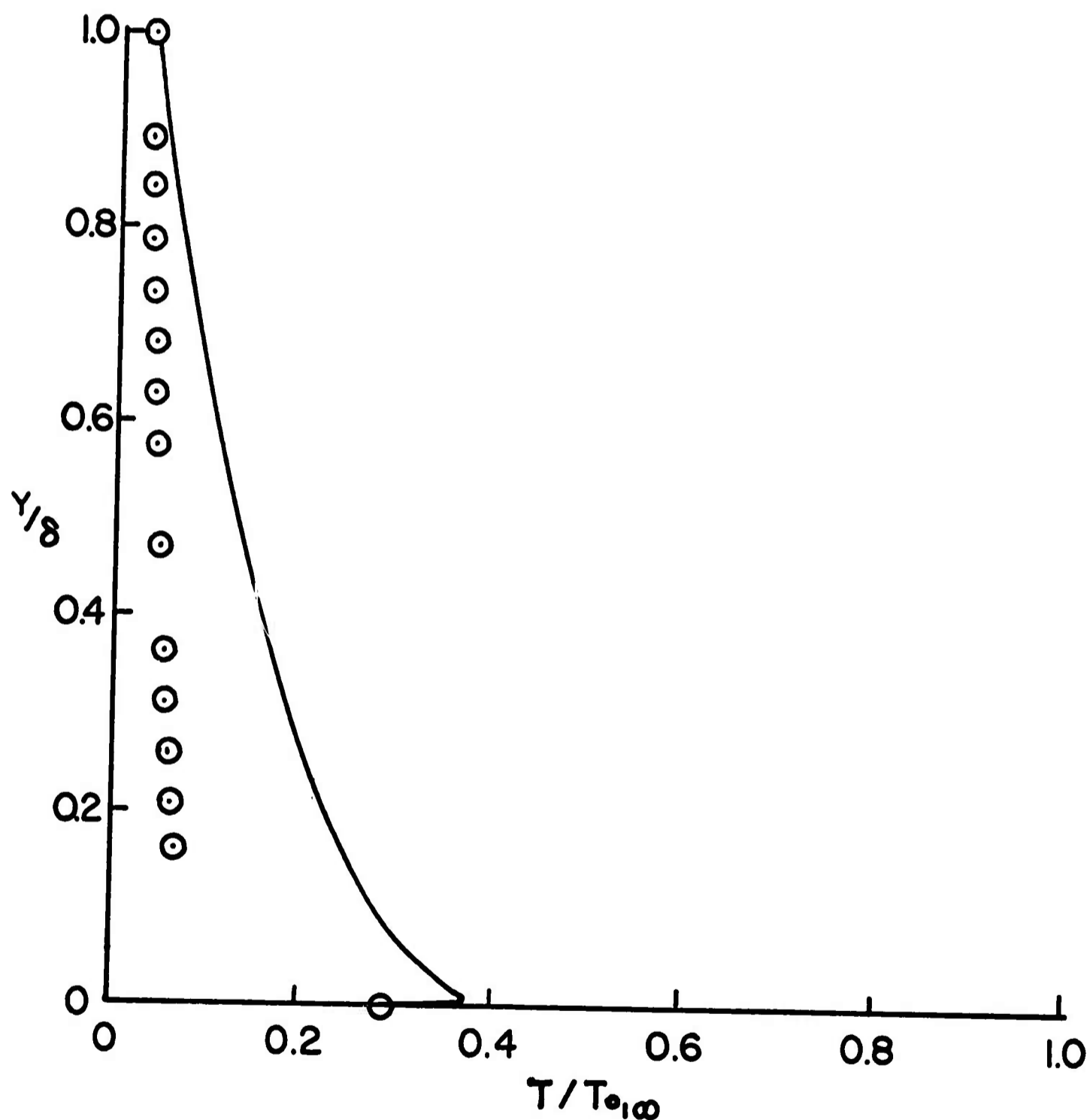


FIGURE 23

COMPARISON OF STATIC TEMP. PROFILE
 AT MACH 11.5

Unclassified

Security Classification

DOCUMENT CONTROL DATA - R&D

(Security classification of title, body of abstract and indexing annotation must be entered when the overall report is classified)

1. ORIGINATING ACTIVITY (Corporate author) Fluid Dynamics Facilities Research Laboratory Aerospace Research Laboratories Wright-Patterson AFB, Ohio		2a. REPORT SECURITY CLASSIFICATION Unclassified	
		2b. GROUP	
3. REPORT TITLE Boundary Layer Profile Measurements in Hypersonic Nozzles.			
4. DESCRIPTIVE NOTES (Type of report and inclusive dates) Scientific Report Internal			
5. AUTHOR(S) (Last name, first name, initial) Scaggs, Norman E.			
6. REPORT DATE June 1966		7a. TOTAL NO. OF PAGES 46	7b. NO. OF REFS 12
8a. FORN DISSEM In-house research		9a. ORIGINATOR'S REPORT NUMBER(S)	
b. PROJECT NO. 7065-0006			
c. 61445014		9b. OTHER REPORT NO(S) (Any other numbers that may be assigned this report)	
d. 681307		ARL 66-0141	
10. AVAILABILITY/LIMITATION NOTICES 1. Distribution of this document is unlimited.			
11. SUPPLEMENTARY NOTES		12. SPONSORING MILITARY ACTIVITY Aerospace Research Laboratories (ARL) Office of Aerospace Research, USAF Wright-Patterson AFB, Ohio	
13. ABSTRACT <p>An experimental investigation made to determine the flow parameter profiles across the boundary layer on contoured, axisymmetric hypersonic nozzles is described. The pitot pressure and total temperature profiles measured across the boundary layers on nozzles of Mach number seven and twelve are shown in graphical form. The static temperature and velocity profiles, calculated with the assumption of constant static pressure across the boundary layer, are given. A correlation is shown to exist between the exponent of the velocity profile power law and the product of the ratios of wall temperature to free stream total temperature and axial distance to momentum thickness. The static temperature profiles, calculated from the measured data is compared with Crocco's relationship for the static temperature in terms of the velocity profile.</p>			

14. KEY WORDS	LINK A		LINK B		LINK C	
	ROLE	WT	ROLE	WT	ROLE	WT
Hypersonic						
Boundary-Layer						
Turbulent						
Nozzle						
Profile-Measurements						
Experimental						

INSTRUCTIONS

1. ORIGINATING ACTIVITY: Enter the name and address of the contractor, subcontractor, grantee, Department of Defense activity or other organization (*corporate author*) issuing the report.

2a. REPORT SECURITY CLASSIFICATION: Enter the overall security classification of the report. Indicate whether "Restricted Data" is included. Marking is to be in accordance with appropriate security regulations.

2b. GROUP: Automatic downgrading is specified in DoD Directive 5200.10 and Armed Forces Industrial Manual. Enter the group number. Also, when applicable, show that optional markings have been used for Group 3 and Group 4 as authorized.

3. REPORT TITLE: Enter the complete report title in all capital letters. Titles in all cases should be unclassified. If a meaningful title cannot be selected without classification, show title classification in all capitals in parenthesis immediately following the title.

4. DESCRIPTIVE NOTES: If appropriate, enter the type of report, e.g., interim, progress, summary, annual, or final. Give the inclusive dates when a specific reporting period is covered.

5. AUTHOR(S): Enter the name(s) of author(s) as shown on or in the report. Enter last name, first name, middle initial. If military, show rank and branch of service. The name of the principal author is an absolute minimum requirement.

6. REPORT DATE: Enter the date of the report as day, month, year; or month, year. If more than one date appears on the report, use date of publication.

7a. TOTAL NUMBER OF PAGES: The total page count should follow normal pagination procedures, i.e., enter the number of pages containing information.

7b. NUMBER OF REFERENCES: Enter the total number of references cited in the report.

8a. CONTRACT OR GRANT NUMBER: If appropriate, enter the applicable number of the contract or grant under which the report was written.

8b, 8c, & 8d. PROJECT NUMBER: Enter the appropriate military department identification, such as project number, subproject number, system numbers, task number, etc.

9a. ORIGINATOR'S REPORT NUMBER(S): Enter the official report number by which the document will be identified and controlled by the originating activity. This number must be unique to this report.

9b. OTHER REPORT NUMBER(S): If the report has been assigned any other report numbers (*either by the originator or by the sponsor*), also enter this number(s).

10. AVAILABILITY/LIMITATION NOTICES: Enter any limitations on further dissemination of the report, other than those

imposed by security classification, using standard statements such as:

- (1) "Qualified requesters may obtain copies of this report from DDC."
- (2) "Foreign announcement and dissemination of this report by DDC is not authorized."
- (3) "U. S. Government agencies may obtain copies of this report directly from DDC. Other qualified DDC users shall request through _____."
- (4) "U. S. military agencies may obtain copies of this report directly from DDC. Other qualified users shall request through _____."
- (5) "All distribution of this report is controlled. Qualified DDC users shall request through _____."

If the report has been furnished to the Office of Technical Services, Department of Commerce, for sale to the public, indicate this fact and enter the price, if known.

11. SUPPLEMENTARY NOTES: Use for additional explanatory notes.

12. SPONSORING MILITARY ACTIVITY: Enter the name of the departmental project office or laboratory sponsoring (*paying for*) the research and development. Include address.

13. ABSTRACT: Enter an abstract giving a brief and factual summary of the document indicative of the report, even though it may also appear elsewhere in the body of the technical report. If additional space is required, a continuation sheet shall be attached.

It is highly desirable that the abstract of classified reports be unclassified. Each paragraph of the abstract shall end with an indication of the military security classification of the information in the paragraph, represented as (TS), (S), (C), or (U).

There is no limitation on the length of the abstract. However, the suggested length is from 150 to 225 words.

14. KEY WORDS: Key words are technically meaningful terms or short phrases that characterize a report and may be used as index entries for cataloging the report. Key words must be selected so that no security classification is required. Identifiers, such as equipment model designation, trade name, military project code name, geographic location, may be used as key words but will be followed by an indication of technical context. The assignment of links, rules, and weights is optional.